Vol. 26 No. 119 *Journal of the Radio Research Laboratories* *March 1979*
Printed in Tokyo, Japan *pp. 13–64*

THE FIRST VLBI EXPERIMENT IN JAPAN

By
Nobuhiro KAWAJIRI, Takeyuki OJIMA, Nobuyuki KAWANO,
Fujinobu TAKAHASHI, Taizo YOSHINO and Kunimasa KOIKE

(Received on November 22, 1978)

CONTENT

ABSTRACT

The first VLBI (Very Long Baseline Interferometry) experiment in Japan was conducted between Kashima (Kashima Branch, the Radio Research Laboratories) and Yokosuka (Yokosuka Electrical Communication Laboratory, Nippon Telegraph & Telephone Public Corporation) by use of respective antenna of 26 m and 12.8 m in diameter during 28 January to 4 February in 1977, after about two years in preparing, and our purpose to establish the first VLBI system in Japan was achieved. The base-line length was about 121 km, and the frequency band was ranging 4180 to 4182 MHz. We received two kinds of radio sources: one from geostationary satellites, ATS-1 and Intelsat IV (F-8), another from celestial bodies such as 3C273B.

We could attain the resolution of 5 ns in determining delay time by the slope of phase spectrum of ATS-1 data. However, the resolution of instrumental delay in measuring was about 10 ns. We could also process the VLBI data of 3C273B by use of the fringe stopping technique.

Several features of the system, and several results are also presented, in which the adequacy of this system was proved.

1. Introduction

It seems that there are high potentiality in VLBI technique which will be available for the various kinds of fields, such as, angular size determination and/or mapping of celestial radio sources, orbit determination of geostationary satellites, geodesy, astrometry, measure-

ment of the earth's rotation and so on. In the RRL (Radio Research Laboratories), some techniques which are indispensable to the establishment of VLBI system have been being developed, such as observation of weak celestial radio sources, very accurate time synchronization, and complicated data reduction procedures. Taking advantage of these techniques, we conducted the first VLBI experiment in Japan between Kashima and Yokosuka during 28 January to 4 February in 1977, after about two years in preparing, and our purpose to establish the first VLBI system in Japan was achieved[1]. Antennas of 26 m and 12.8 m in diameter were used at the respective site, and the used frequency band was ranging 4180 to 4182 MHz. The simplified block diagram of our VLBI system is shown in Fig. 1.

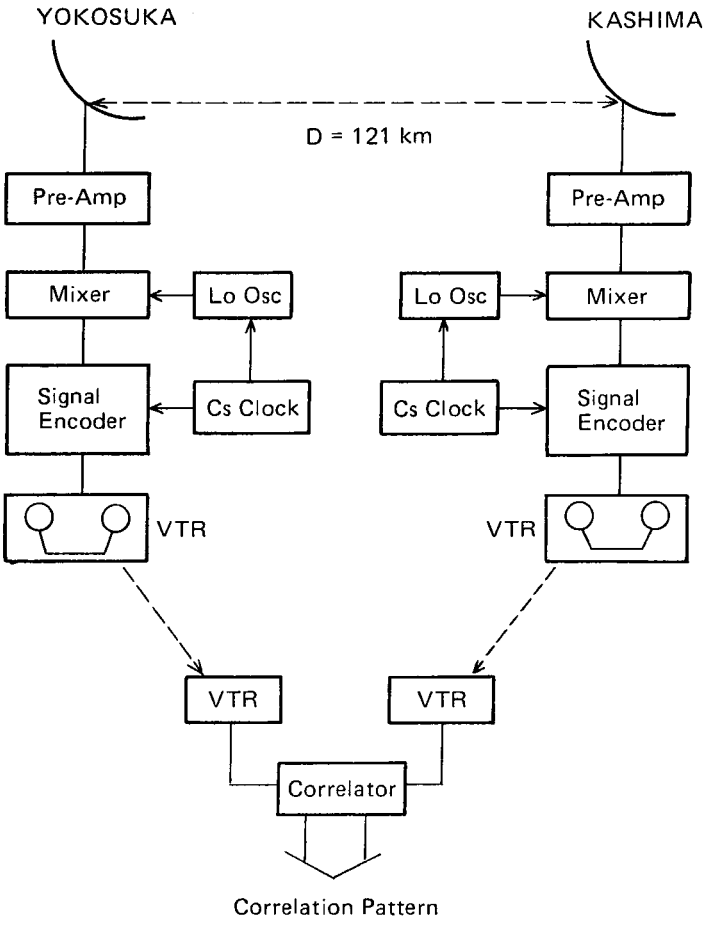

Fig. 1 Simplified block diagram of our VLBI system

We utilized two kinds of radio sources: one from geostationary satellites, ATS-1 and Intelsat IV (F-8), another from celestial bodies, 3C84, 3C273B and 3C454.3.

The radio noise from satellites which was due to thermal noise of TWTs (Travelling Wave Tube) in the satellites, was so intensive that the data of them were easily processed, and we could attain the resolution of 5 ns (nano second) in determining delay time by the reduction of ATS-1 data. Although the intensities of celestial radio sources were lesser than

those of satellites, on the other hand, we could process the data of 3C273B so far by use of the fringe stopping technique.

In the subsequent chapters, the whole system and the processing of the experimental data are described in detail with regard to each part. In chapter 2, frequency stability of local oscillator system, recording and reproducing, correlation, time synchronization, and instrumental delay measurement are considered. In chapter 3, descriptions on radio sources in the experiment with its practical procedures are given. In chapter 4, theoretical background for VLBI data processing is mainly given, and processing data by both of satellite and celestial radio source is also explained. In chapter 5, some problems occurring in the course of establishment of this VLBI system are discussed, and in chapter 6, the results which were obtained from this VLBI experiment are given.

From these results the orbit determination of satellites and the detection of phase scintillation were also tried, the details of which are described elsewhere.(2)(3)

2. The Whole System

The whole system of our VLBI experiment is shown in Fig. 2. The system was developed, by being partly referred to the Mark II system which is frequently used in the U.S.A. and European countries, by using VTR and consequently adopting digital diphase coding, and receiving bandwidth of 2 MHz. However, other parts of the system were significantly different from those of Mark II, in both hardware and software, and also in making bandwidth narrower by 200 kHz. We tried to construct this system, utilizing the existing apparatuses and equipments in the RRL as far as possible.

2.1 Antenna, Feed, and Local Oscillator Systems

2.1.1 Antenna and Feed Systems, and Preamplifiers

The antenna at Kashima is a Cassegrain type reflector of 26 m in diameter, and its primary feed forms a conical horn reflector. The polarization of received radio wave was linear. As a preamplifier, uncooled parametric amplifier is used and the system noise temperature is kept to be about 110 K for this VLBI experiment.

Though the electrical performance of Yokosuka antenna is similar to that of the Kashima antenna, there are some differences as follows. Its diameter is 12.8 m and the axis of main dish is separated by 1.8 m from the azimuth rotation axis, due to the two-reflector beam guide feeding system (see Fig. 3). Any one of radio waves of either linear or circular polarization can be received.

In the VLBI experiment, we utilized the linearly polarized wave.

2.1.2 Local Oscillator System

In the practical signal processing of VLBI, frequency stabilization of the local oscillator in the receiver brings about the most important problem. Its theoretical explanation is given in 2.1.3 and 4.1, and we describe here the actual system in which the received signal on 4180 MHz is down-converted to the video one (2 MHz bandwidth) and clipped to NRZ (non-return-to-zero) signal.

The block diagram of the receiving system is referred to Fig. 2. In order to obtain the frequency of 4110 MHz in the first local oscillator, 5 MHz output from a Cs frequency standard is fed into the universal synthesizer, HP5100B at Kashima and HP5105A at

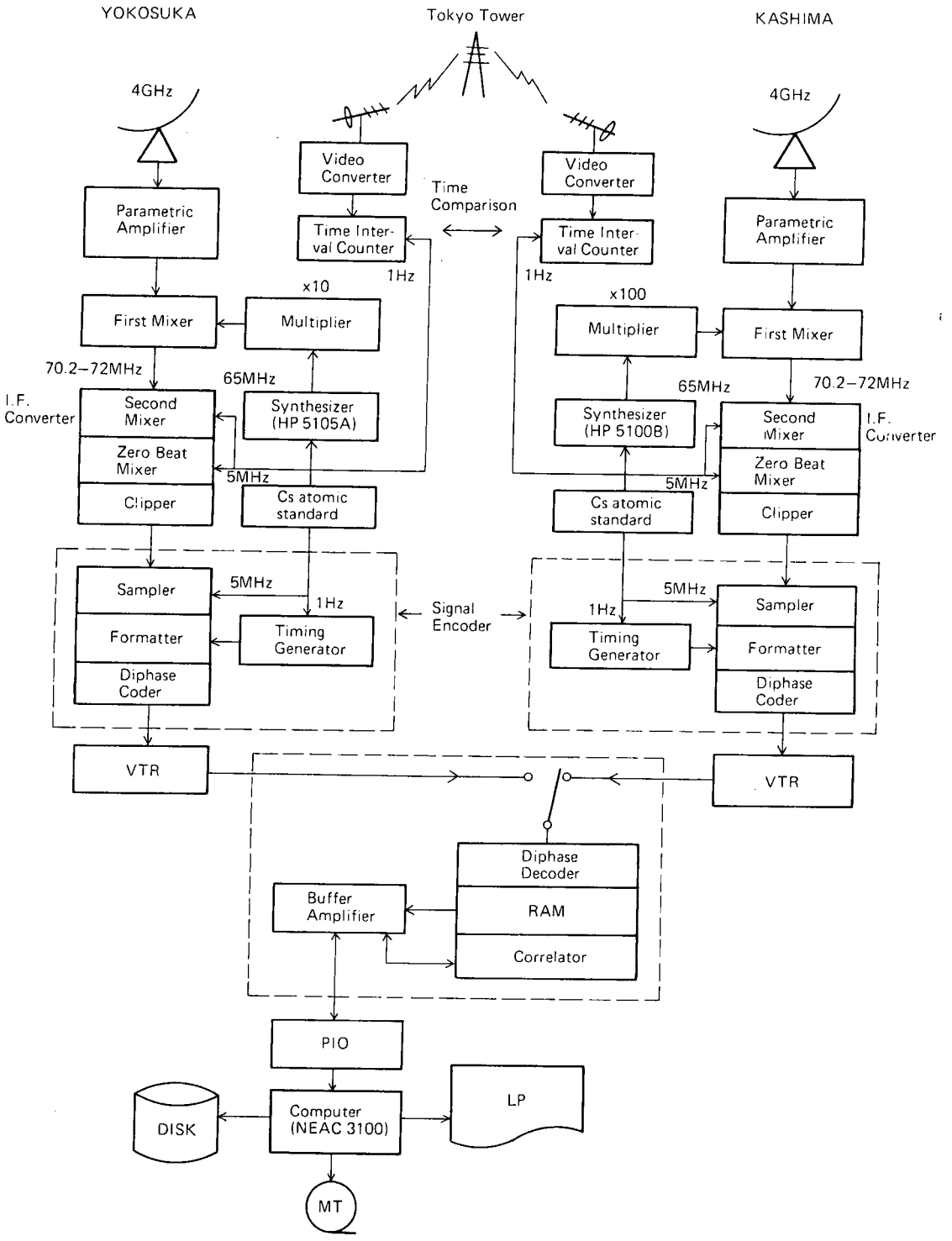

Fig. 2 Whole system of our VLBI experiment

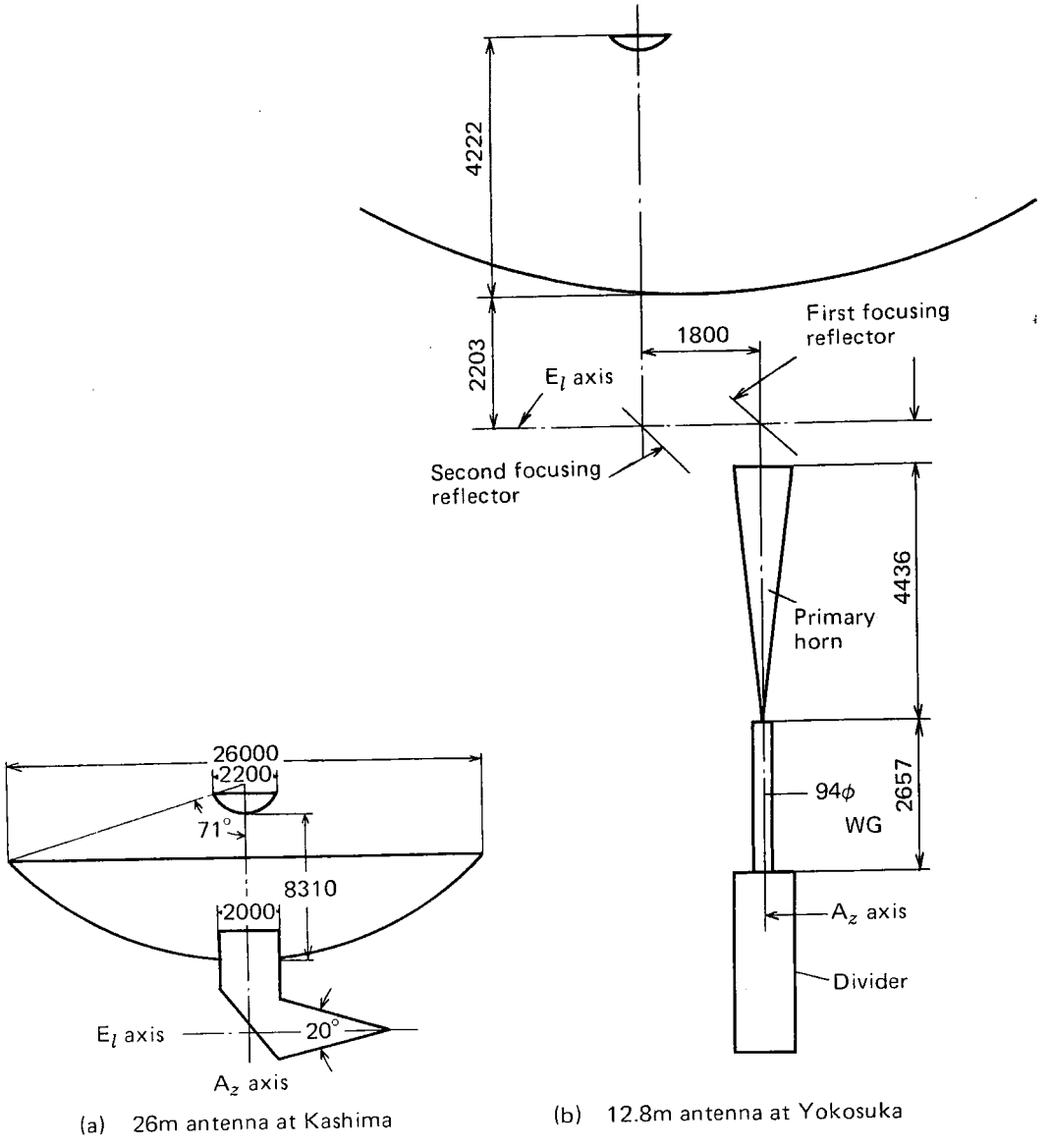

Fig. 3 Dimensions of antenna and feed system at Kashima (a) and at Yokosuka (b)

Yokosuka, and then multiplied. According to the synthesizers used, multiplication factor attained 100 at Kashima and 10 at Yokosuka, respectively. Local oscillator signal of I.F. converter was produced also by the Cs frequency standard. In the I.F. converter, the signal frequency is again down-converted from 70.2 ~ 72 MHz IF signal to the 0.2 ~ 2 MHz video signal cutting image one. In this process, the signal is mixed twice with the second and third local oscillator frequencies of 65 and 5 MHz, respectively. The signal is taken out finally in the shape of NRZ signal with the level of ±0.3 V. The clipped NRZ signal stands for the zero-cross of the input random noise almost correctly, that is, to the extent of more than 99 percent in time sequence (see Fig. 6).

2.1.3 Frequency Stability

The received signals at the two antennas from the same radio source are correlated. To consider this relation to the VLBI system, extremely stable signal is needed for the independent local oscillators, when a local oscillator signal can not be available in common. Frequency stability needed is dependent on integration time[4], which is closely concerned with the S/N ratio of the received signal. Fortunately, the flux intensity of artificial satellite was so strong that the integration time of about 1 ms was enough to process the data. However, in case of radio star, the integration time more than 1 sec is needed. Furthermore, in case of receiving weaker radio star, several minutes or several hours of integration time must be necessary.

In order to limit phase fluctuation of local oscillator signal less than 1 radian during the integration time, frequency stability better than $10^{-12} \sim 10^{-13}$ is necessary. As only Cs frequency standards of HP Model 5061A were available in this experiment, the stability of local oscillator system was examined before the experiment, concerning to the multiplier, the frequency synthesizer, and the total system. In Fig. 4, the measured stabilities of some combinations among them and of those given in the catalogue are shown. In this figure,

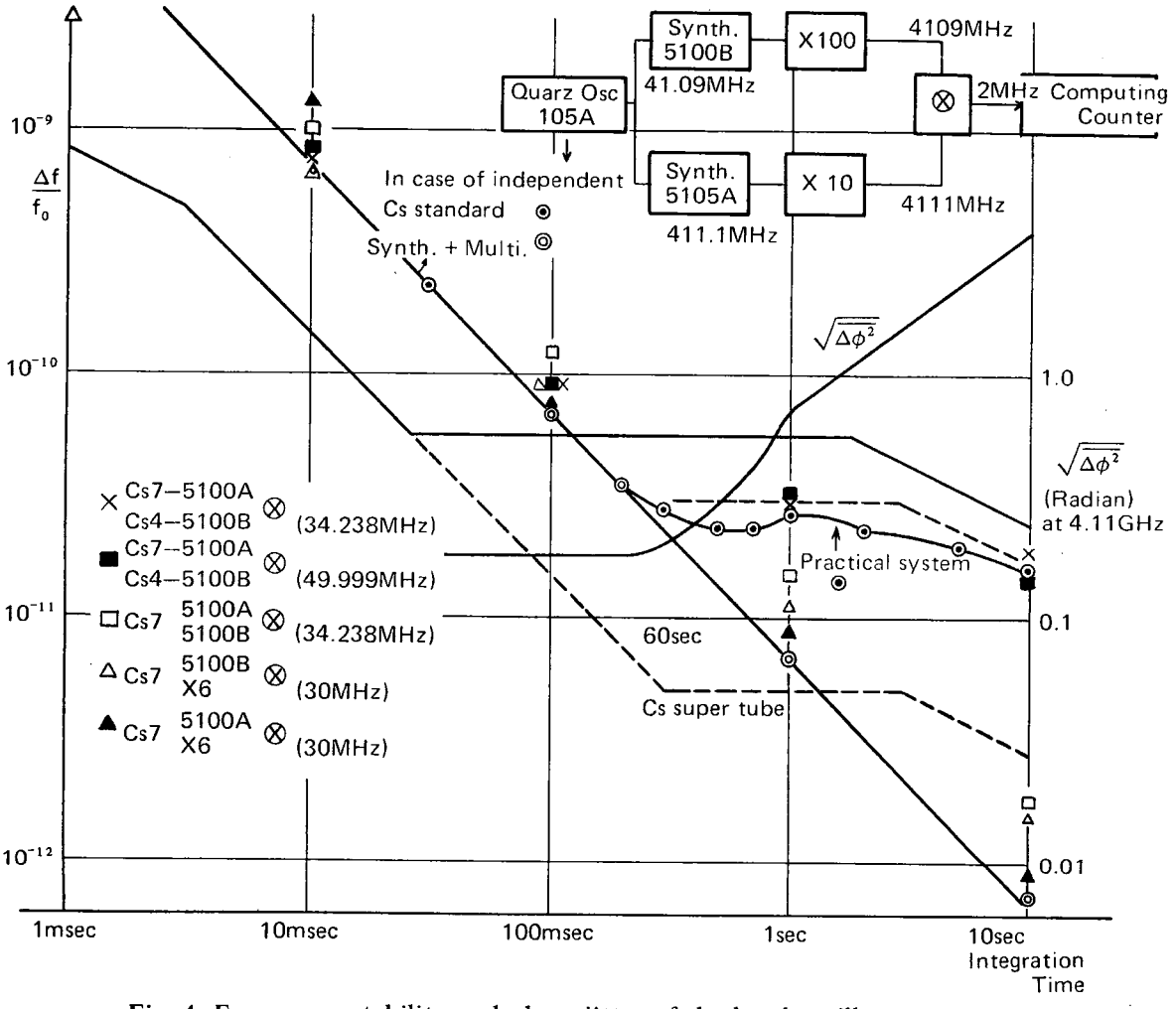

Fig. 4 Frequency stability and phase jitter of the local oscillator system

converted phase fluctuation value at 4110 MHz is also shown by the right-hand scale. In order to measure the baseline length more precisely in the geodetic application, it is necessary to make the phase fluctuation lower[5]. As is shown in Fig. 4, if we accept phase fluctuation of one radian, integration time of about 2 sec is possible in our system. Effective frequency stability is apt to be worse in the short integration time region when frequency synthesizer and frequency multiplier are used.

In general, phase fluctuation, $\Delta\phi$, relates to the frequency stability as in the following equation, on the assumption that the fluctuation is due to white noise in frequency:

$$(\Delta\phi)^2 = \omega_L{}^2 \sigma_y{}^2 \tau^2, \quad \cdots\cdots\cdots\cdots\cdots\cdots\cdots\cdots\cdots\cdots\cdots\cdots\cdots\cdots\cdots\cdots \quad (1)$$

where ω_L : angular frequency of the local oscillator,
$\Delta\phi$: phase fluctuation (r.m.s.) due to instability,
σ_y : frequency stability ($= \Delta f_{r.m.s.}/f$),
τ : integration time (averaging time).

On the other hand, the square of the phase fluctuation derived from S/N ratio is almost inversely proportional to the S/N ratio, as shown below[6],

$$(\Delta\phi)^2 \propto \frac{\sqrt{T_{S1} \cdot T_{S2}}}{\sqrt{T_{A1} \cdot T_{A2}}} \cdot \frac{1}{\sqrt{B\tau}} \propto \frac{1}{S/N}, \quad \cdots\cdots\cdots\cdots\cdots\cdots\cdots\cdots\cdots\cdots\cdots\cdots\cdots\cdots \quad (2)$$

where T_{A1}, T_{A2} : antenna temperature by the radio source,
T_{S1}, T_{S2} : system noise temperature,
B : frequency bandwidth.

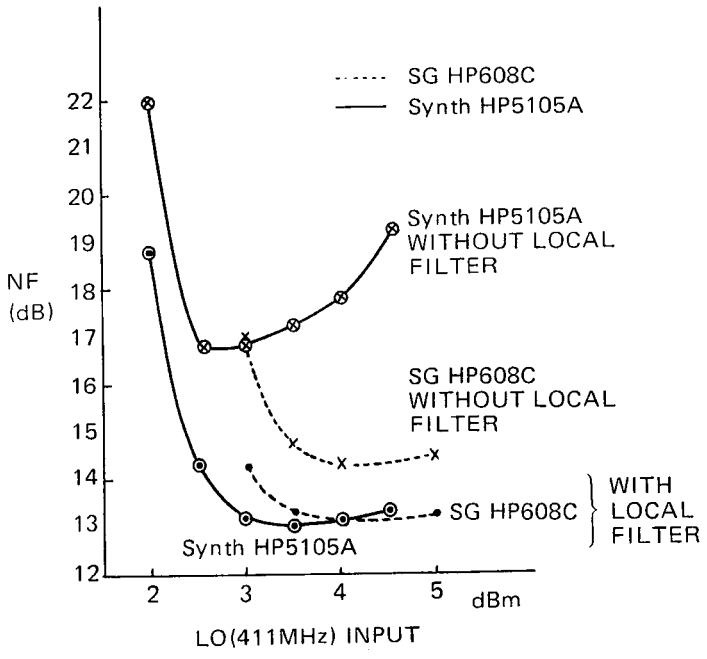

Fig. 5 Noise Figures using synthesizer HP5105A and signal generator HP608C as a local oscillator

Since this kind of phase fluctuation related to S/N ratio is connected with the data processing, system noise temperature must be decreased in the receiver. Phase noise proper to local oscillator system, which also increases the system noise temperature, grows in proportion to the square of multiplication factor. In our system, therefore, in order to reject the high frequency component of such phase noise, the final output of multiplier was filtered by a narrow BPF (Band Pass Filter). Thus, the noise figure of the receiver system was improved by 4 dB. Fig. 5 shows this situation. It may be clear that the noise figure of synthesizer used as a local oscillator is apparently less than that of signal generator.

Short term phase jitter due to the parametric amplifier was measured to be less than 5°p-p. So it could be neglected.

2.1.4 Clipped Noise Signal

Before the process of one bit sampling, it is desired to perform the extreme clipping. We determined the gain of the clipping amplifier so as to clip the noise signal waveform of 0.2 ~ 2 MHz bandwidth, to the extent more than 99 percent in time sequence at the system noise level. If type of noise is gaussian, the time ratio, F(x), that noise waveform exceeds the clipping voltage, V_C, is expressed as follows,

$$F(x) = \frac{1}{\sqrt{2\pi}} \int_x^{\infty} \exp\left(-\frac{x^2}{2}\right) dx, \quad \cdots\cdots\cdots\cdots\cdots\cdots\cdots\cdots\cdots\cdots\cdots\cdots\cdots\cdots\cdots\cdots\cdots\cdots \quad (3)$$

where $x = V_C/V_e$,

V_e : rms voltage of random noise.

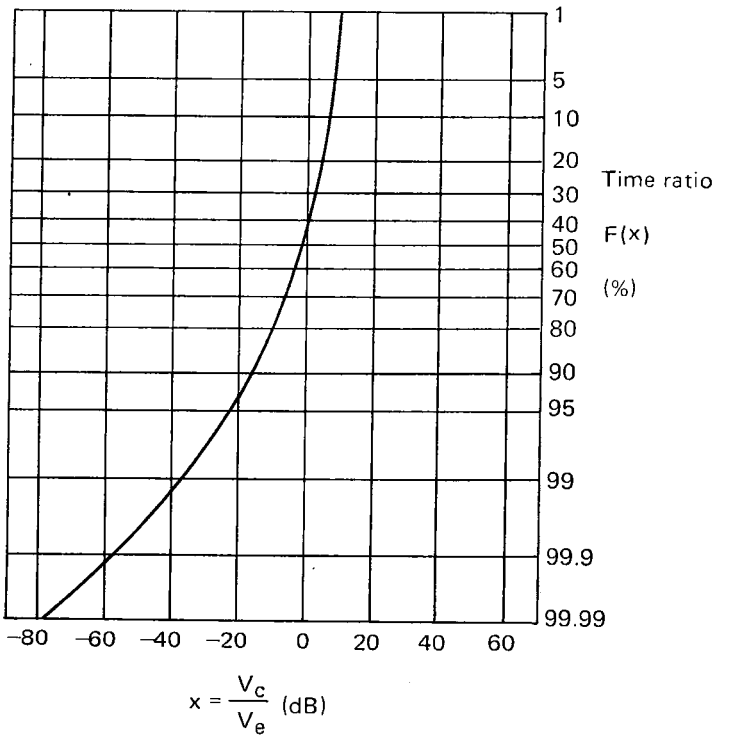

Fig. 6 Percentage of time during which the voltage ratio exceeds $x(=V_C/V_e)$

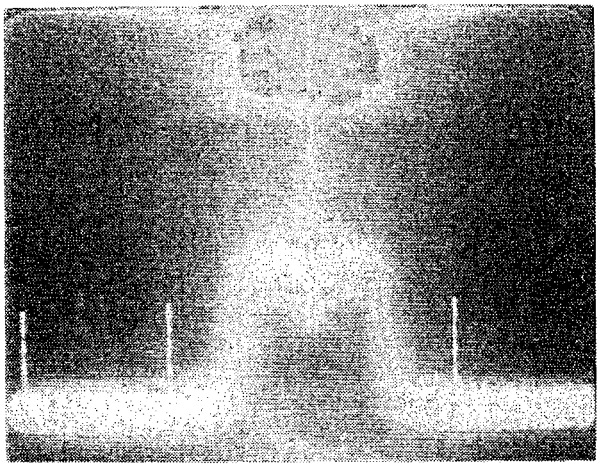

Fig. 7 Spectrum of the signal before clipping

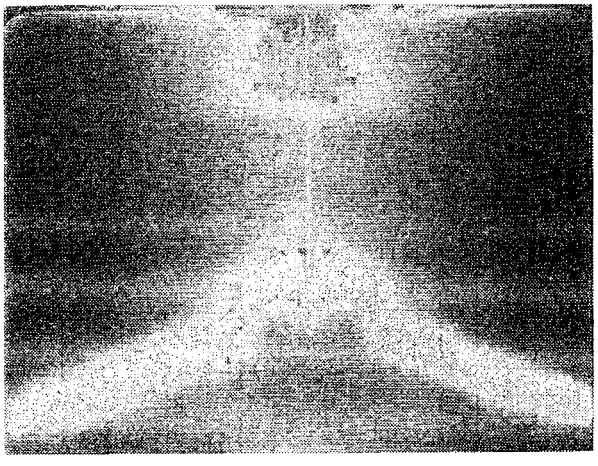

Fig. 8 Spectrum of the signal after clipping

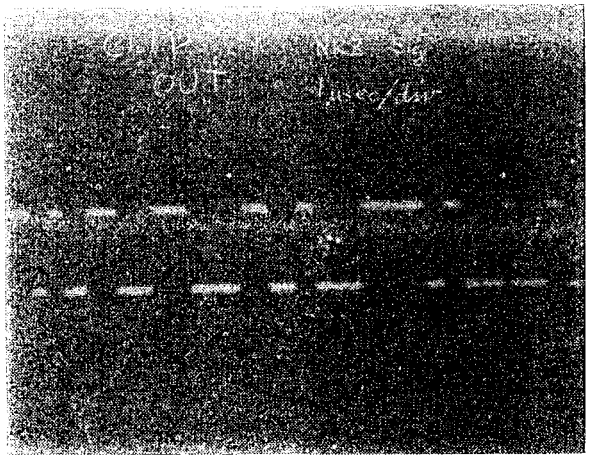

Fig. 9 NRZ signal clipped

The function F(x) is shown in Fig. 6. In this graph, V_c must be lower than one hundredth of V_e. The spectrum before the clipping is shown in Fig. 7, and the spectrum after the clipping is also shown in Fig. 8. In these figures, one can see that the spectrum of random noise waveform after the extremely clipping expands in triangular shape in the neighborhood of the band. This fact is, even quantitatively, coincident with the results calculated by Van Vleck and Middleton[7]. Finally, a picture of NRZ signal clipped is shown in Fig. 9.

2.2 Recording and Reproducing

2.2.1 Outline on Signal Encoder and VTR

As is shown in Fig. 9, output signal from I.F. converter is the clipping NRZ signal. In order to digitize the signal, it was sampled in a signal encoder with the clock based on Cs atomic standard. The data were one-bit sampled and transmitted to recording system continuously. As the receiving bandwidth was having about 2 MHz in this experiment, VLBI data were sampled at the rate of 4 Mbps. The data were generally treated at off-line processing. So, a tremendous quantity of data must be recorded in a mass memory. Though the cost of such a digital memory is rather high, VTR can be obtained at fairly low cost, and has advantages of comparatively wideband and of large analog memory. Thus a re-modeled VTR (TOAMCO VR 489DR) was utilized in our experiment.

The VTR consists of recording heads of a helical scanning type and of a half inch wide tape. FM modulator in a VTR improves the S/N ratio, but it limits the recording bandwidth. So, direct recording method was used, which yielded comparatively wideband recording (cf. Fig. 10). The second harmonic of 4 MHz signal was recorded sufficiently.

The data, record control signal, and time index which is generated by the time signal generator were arranged according to the recording format, and these bit arrangements were also made in the signal encoder. The format used is shown in Fig. 11. Since tape recorder always has small quantity of wow and/or flutter movement, so-called digital diphase coding was adopted in order to minimize the effects of wow and flutter. When recorded data were reproduced, the signal was digitally diphase-decoded in the correlator.

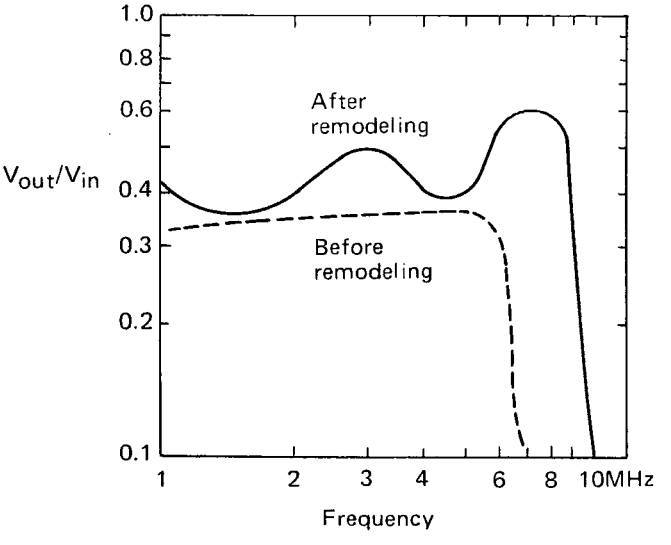

Fig. 10 Frequency characteristics of VR 489DR

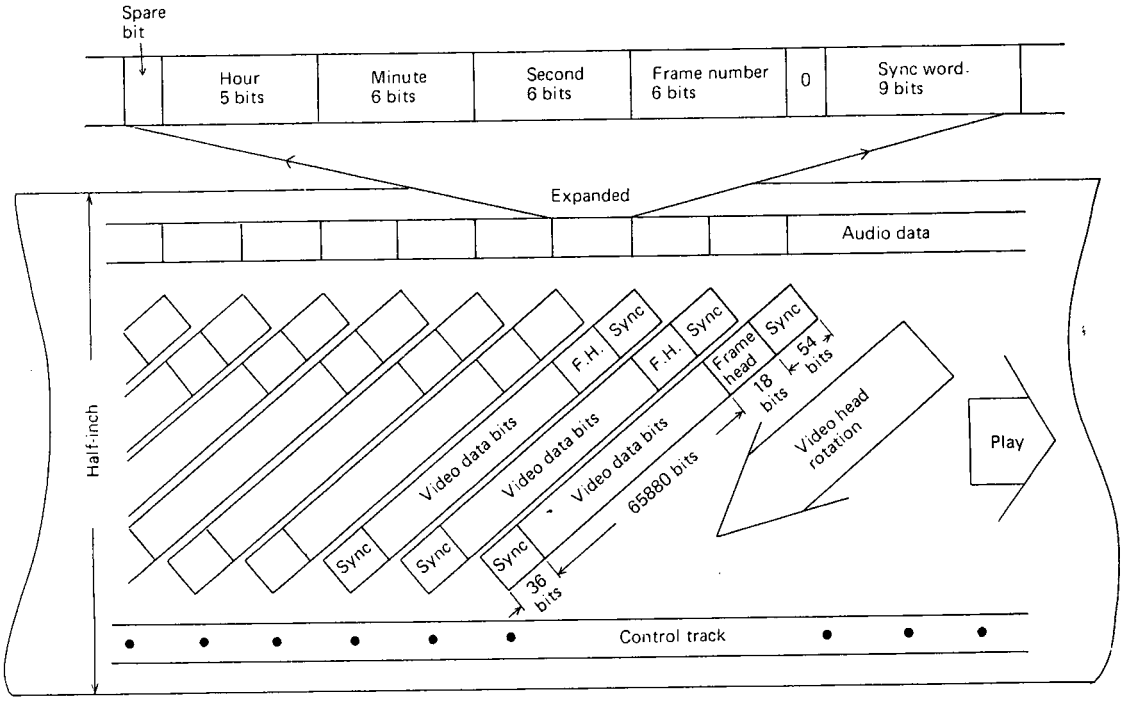

Fig. 11 Recording status on magnetic tape of VTR

2.2.2 Signal Encoder

The function of signal encoder is related to the recording procedure. Generally, reproduced analog signal from the magnetic tape is not always equal to the recording signal, because of unflatness of power and phase characteristics of recording apparatus in the band, and of difference of tape speed at the time of recording and reproducing. The former problem is solved by adapting an amplitude and a phase equalizer or by digitizing signals. However, the latter problem would be solved by using the instrument which has quite good quality in servo system. If the VTR had another video-recording track, clock signal could be recorded simultaneously, and accurate signal reproducing could be done by this clock signal, which could cancel the variation in tape speed. Unfortunately VTR has one video track and one audio track as usual. The former can record several Mbps, but the latter can record only several kbps, so clock signal cannot be recorded simultaneously. However, if the signal modulated by the clock signal is recorded, the recorded signal can be reproduced properly. Therefore we adopted the digital diphase-coding mentioned later.

The functions of signal encoder are as follows:

1. sampling and digitizing
2. affixing a time index
3. digital diphase-coding (modulation)
4. formatting

Explanation on these functions and actual instruments is described below.

2.2.3 Missampling

In our system one bit sampling with 4 Mbps was used as the usual VLBI recording system. In one bit sampling, when the signal level stays between positive and negative thresholds, it is not always sampled correctly, which we call missampling. Even if we use the amplifier whose gain is infinitive to minimize the probabilities of staying of the signal in the neighborhood of 0 V before sampling, the output signal is still unsatisfactory being clipped together relating to the internal noise in the amplifier. Moreover, since practical amplifier has finite bandwidth, the rise time and fall time of clipped signal cannot be zero. So it is not completely possible to avoid missampling. Fig. 12 explains the cause of the missampling. When missampling happens frequently and the missampled signal is taken out as 1 and/or 0 randomly, S/N ratio decreases. When the output signal is biased, input signal is considered to have DC component. The former case is not so serious because they are cancelled within a long time, but in the latter case, the accuracy of measurement is lowered, and this must be

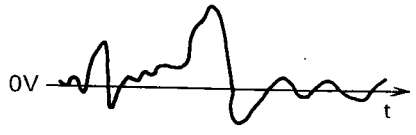

(a) Input signal

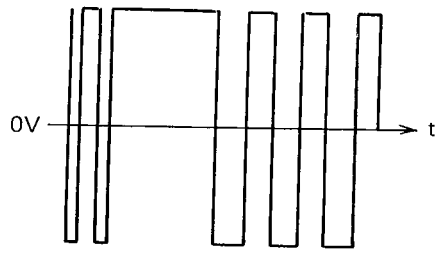

(b) Clipped signal after amplification with infinitive bandwidth and gain

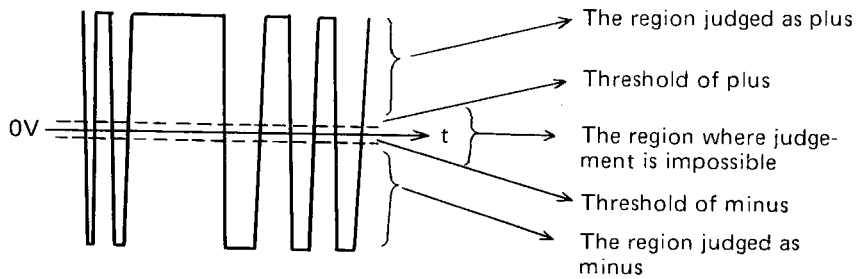

(c) Clipped signal after amplification with practical device

Fig. 12 Explanation of the cause of missampling

avoided. The frequency of missampling is shown below theoretically. As the input signal is carrying random noise, the probability of signal level, p(V) dV, to stay between V and V+dV in voltage, is expressed as[8],

$$p(V)\,dV = [1/\sqrt{2\pi V_{eff}^2}]\cdot\exp[-V^2/2V_{eff}^2]dV, \quad \cdots\cdots (4)$$

where V_{eff}^2 is the mean square value of V^2

Amplifying this signal by voltage gain, G, the probability for signal level to stay between $-V_0$ and $+V_0$ in voltage becomes

$$P(V_0) = \int_{-V_0}^{V_0} (1/G\sqrt{2\pi V_{eff}^2})\exp(-V^2/2G^2V_{eff}^2)dV \simeq 2V_0/G\sqrt{2\pi V_{eff}^2}, \quad \cdots\cdots (5)$$

where G is considered to be large enough.

When V_0^2 is equal to V_{eff}^2 and G is 20 dB, $P(V_0)$ is calculated as 0.8 percent and this value is in negligible order.

If the amplifier has 0 ~ 100 MHz bandwidth and the pulse wave form as in Fig. 9 is supplied, the time during which the signal level stays between two thresholds in Fig. 12 is estimated as about 5 ns. The number of zero crossing in 1 sec of time, P_0, is given by the next relation,

$$P_0 = 2\left[\int_0^\infty f^2 w(f)df \Big/ \int_0^\infty w(f)df\right]^{1/2} \simeq 1.155\ B, \quad \cdots\cdots (6)$$

where w(f) : normalized power spectrum,
B : bandwidth of input signal (B ≃ 2 MHz).

Since the transition time between two thresholds is about 5 ns, and the number of zero crossing is 1.155 B, the probability of missampling is about 1 percent and is also negligible.

2.2.4 Digital Diphase Coding in Signal Encoder[9]

Since the recording bandwidth of the VTR is limited and clock signal must be recorded as the video signal, it is desired that quantity of data or bit rate becomes minimal. Digital diphase coding is appropriate for this purpose.

The procedures to derive the 4 MHz clock pulses and the original NRZ signal from diphase coded data are described in 2.2.7 (2).

2.2.5 Timing of Sampling

Incomplete synchronization in sampling timing at both antenna sites is equivalent to the change of total delay time, τ. As the experiment needs several nsec resolution, jitter of sampling pulse must be limited to less than several ns. Sampling pulse lacking of sharp leading edge causes inaccurate sampling timing, so the rise time must be as short as possible. Further, change of the waveform of sampling pulse due to the temperature variation may be equivalent to the phase jitter of the sampling pulse. So the circuits of the sampler and the sample pulse generator must operate fast, and must be freed from the effect by the change

of the environmental conditions.

Even if the jitter of the sampling pulse occurs, no trouble is introduced under the conditions that the mean interval of the pulse is constant along the time sequence in synchronization to each atomic standard. The time synchronizing error must be measured separately.

2.2.6 Composition of Signal Encoder

Signal encoder consists of 6 components, which are shown in Fig. 13. Each component except display is described here.

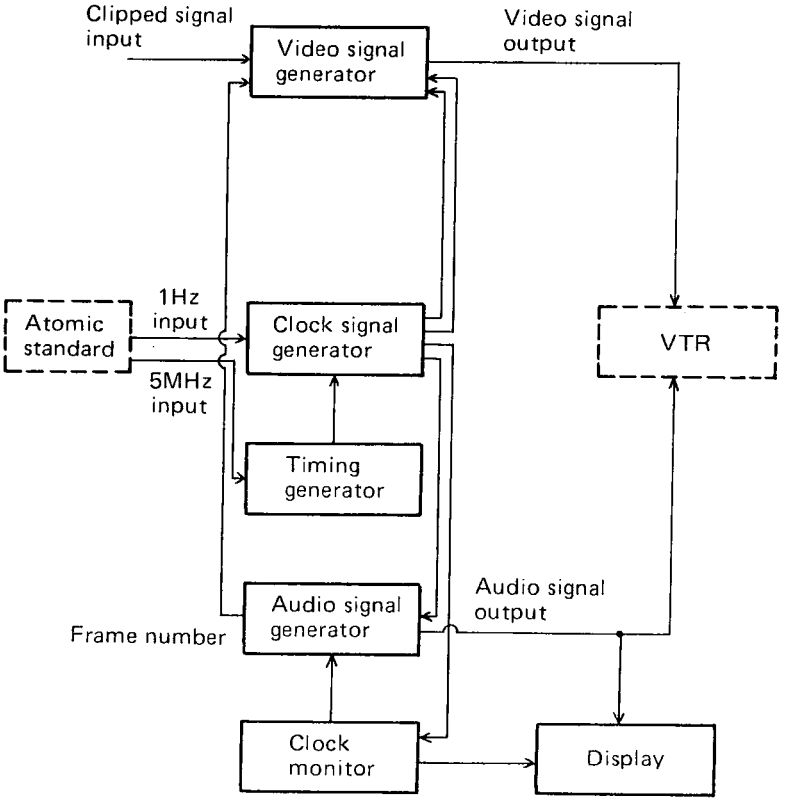

Fig. 13 Block diagram of signal encoder

(i) Timing generator

Timing generator produces 24 MHz signal on which all the frequency used in a signal encoder is based, and it consists of VCXO (Voltage Controlled Crystal Oscillator) and automatic phase controller. The 24 MHz VCXO output is phase-locked to the 5 MHz output of the Cs atomic standard. The 24 MHz output varies within ±5 ns which is the same amount as the resolution of delay time. The block diagram is shown in Fig. 14.

(ii) Clock signal generator

Clock signal generator produces all the frequency used in a signal encoder and they are listed in Table 1. Since VTR switches its recording head once every 1/60 second, we handle the data for 1/60 sec as one frame. 60 (0 to 59) frames of data, affixed 0 to 59 number of

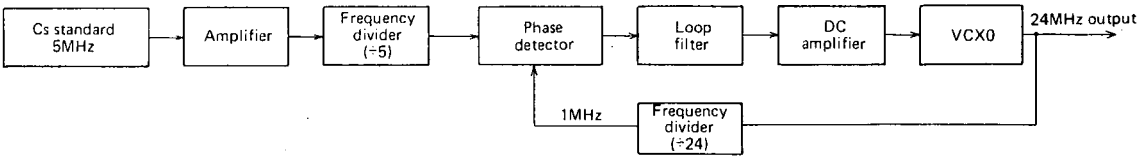

Fig. 14 Block diagram of timing generator

frame, are distinguished each other, and the number of bits in a frame is 66666 (for Fr. No. (Frame Number) of a multiple of 3) or 66667 (for Fr. No. of non-multiple of 3). Tape speed and head rotating speed of VTR is stabilized by the drive-synchronizing pulse of 60 Hz which is based on the 24 MHz, as written in Table 1.

Table 1 Frequencies utilized in the signal encoder, and purposes

Frequency	The purpose
8 MHz	Diphase coding of video data
4 MHz	Sampling and video data output
2.66 MHz	Synch-word
4 KHz	Diphase coding of audio data
2 KHz	Audio data output
60 Hz	Time interval of a frame, and VTR drive synchronization pulse
20 Hz	Judgement of the frame number whether it is a multiple of 3 or not
1 Hz	Time synchronization

(iii) Video signal generator

Video signal generator samples the clipped signal of 2 MHz bandwidth, arranges the time index and the data in a bit stream according to the format, and puts out these bit stream to the VTR after diphase coding. The format of video data is shown in Fig. 15. In this figure, synch-word means the marker of the start or stop of the frame. These are used at the reproducing, for the beginning and the end of memorization of the data by detecting these synch-words.

In this system, missampling is dealt with as follows. At first the input signal is wave-shaped by high speed comparator in order to minimize duration for voltage level to stay between the thresholds, which gives the uncertain level of "1" or "0". If two samplers which are to work simultaneously in the signal encoder give different levels with each other, that is "1" and "0", the sampler works to put out "1" and "0" alternately. Thus the miss-amplings are dealt as a kind of internal noise in the long-time averaging.

(iv) Audio signal generator

Audio signal generator codes a time mark and a misclock (cf. next paragraph (V)) in the signal encoder, and takes out them after diphase coding. Bit rate of the audio data is 2 kbps, and one frame consists of 34 bits (for Fr. No. of a multiple of 3) or 33 bits (for those of non-multiple of 3). The format of audio data is shown in Fig. 16.

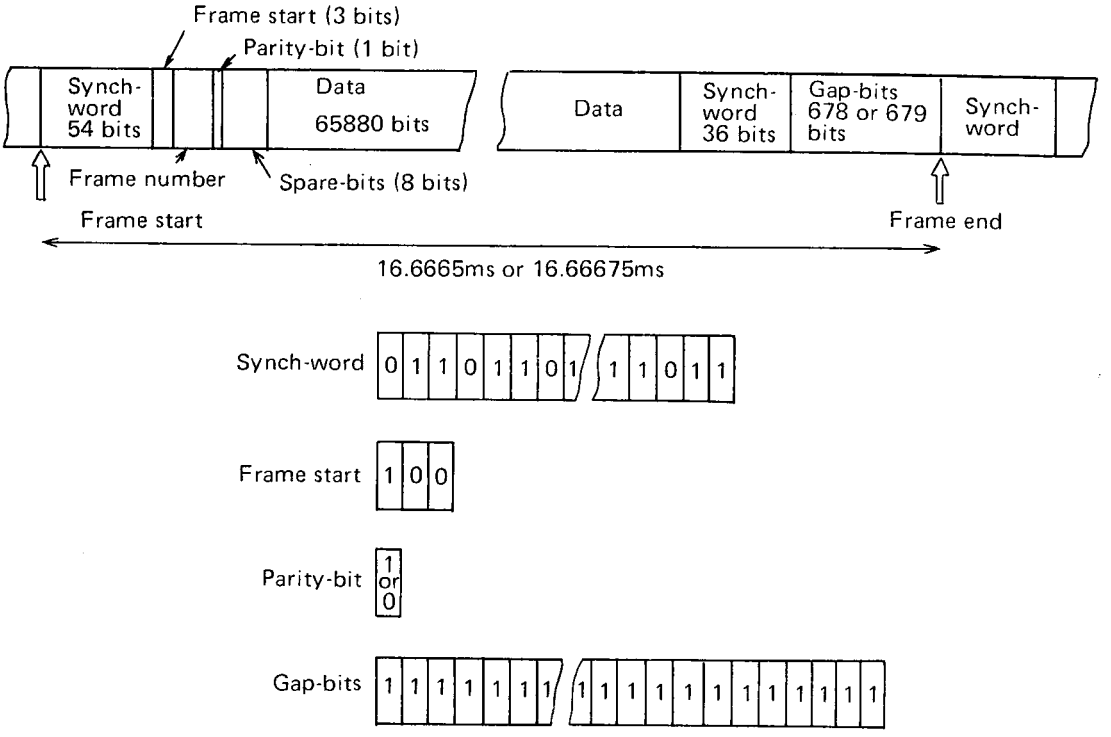

Fig. 15 Video data output format

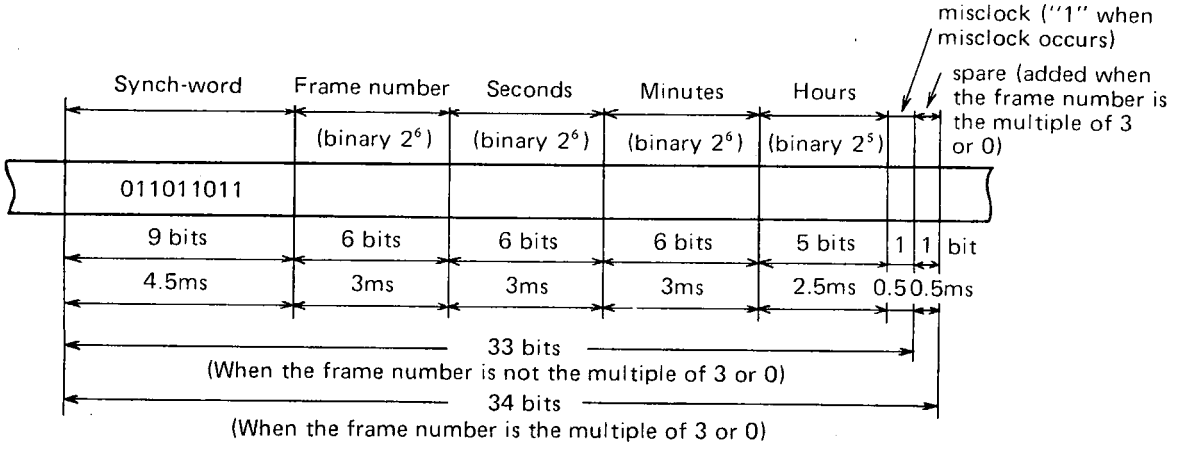

Fig. 16 Audio data output format

(v) Clock monitor

The loss of 1 bit causes delay time error of 250 ns, to which attention must be paid. As the loss of data occurs mainly by the loss of sampling pulse which is called misclock, 4 MHz clock must always be watched. When misclock occurs, it is recorded as an audio datum and an alarm is given.

As the lag in timing of each sampling, that is, the time synchronization error deteriorates the data in determining the delay time, 1 pps signal from the 24 MHz clock and that from the Cs atomic standard are always compared with each other. When the synchronization is lost, this is also recorded as an audio datum.

2.2.7 VTR Recording and Reproducing

(1) VTR recording

We used VTR, TOAMCO-VR489DR, to record the one bit sampling data from the signal encoder. The specification of this VTR is shown in Table 2. As mentioned in 2.2.1, this VTR was remodeled to expand the bandwidth of video recording to fit the experiment. The first point of remodeling is placed on the recording modulation techniques, namely, we adopted the direct recording instead of the ordinary frequency modulation. The second point is placed on the complete remodeling of the equalizing amplifiers and the recording current amplifiers to make VTR hold wider band. These two remodeling give us the 9 MHz video bandwidth (3 dB down) as shown in Fig. 10. However, these remodeling bring some ripples near 3 MHz and 7 MHz. Expansion of bandwidth is incompatible with decreasing of ripples, and we preferred the bandwidth expansion to the reducing of ripples in this case.

Table 2 Specifications of VTR VR-489DR

Video bandwidth	10 kHz -- 9 MHz
Audio bandwidth	70 Hz -- 10 kHz
Wow & flutter	within 0.3% (rms)
Synchronization	composite & external capstan servo system
Drive control	local & external

(2) Digital diphase CODEC (coding and decoding)

Fig. 17 illustrates the digital diphase codec[9]. The first line, line A, is a typical data pattern in which high level means one in binary code. The next line B is the diphase representation of the same data. In the diphase coding, there is a transition always at every 250 ns interval. When the data are kept at high level, additional transitions take place in the middle of the bit interval.

The process of data recovery is shown in the following lines. The next step is to make the signal delay by 250 ns to get line B′. Then line B and line B′ are multiplied by a logic exclusive NOR. This logical product is shown in line C, which is identical to line A, original data, except a delay.

The next step is one scheme of recovering clock from the diphase data. Line D presents the negative and positive transitions on an edge detection of line B′, and all the edge comes out as a narrow spike.

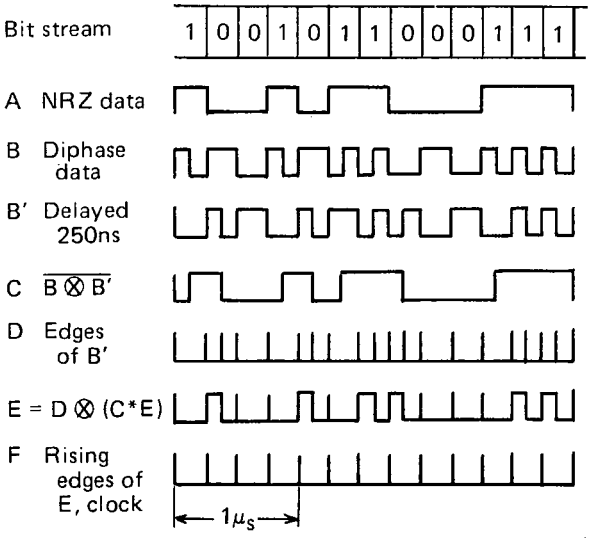

Fig. 17 Schematic diagram of diphase coding

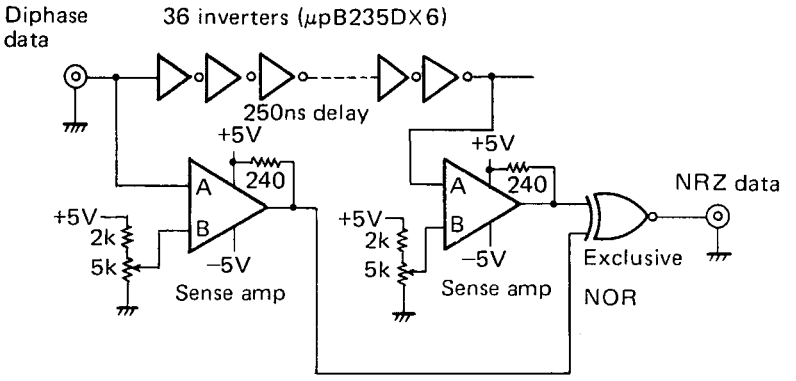

Fig. 18 Decoding circuit of diphase data

The line C data can be used to gate out the extra pulses using a feedback logics of next equation, and we get line E

$$E = D \otimes (C * E),$$

where a mark ⊗ represents exclusive OR logic and a mark * represents AND logic. After differentiation of line E, desired clock pulses comes out as line F.

In our correlator, the delay of 250 ns between B and B′ is made by thirty six serial TTL inverters and the circuit of these logics is shown in Fig. 18.

(3) Synchronization between video and audio frames

Fig. 11 shows our recording format on video tape. The time codes, that is, hour, minute, second, and frame number are recorded on an audio track and high speed sampling data are recorded on a video track. The recording speed of audio track is 2 kbps and that of video track is 4 Mbps.

Diphase coding was applied to both the audio and video data. Also, in the audio track

we recorded the negative 60 Hz pulses synchronized with atomic clock to use them as timing clocks for the servo synchronization, on reproducing the VTR data.

Both video and audio data have sync-words at the head of each frame in order to keep the frame synchronization at the reproduciton, because the capstan servo system of VR-489DR does not absorb the tape's flatter. This flatter causes the change of tape length between an audio and a video head, and makes time lag of a few ms in both data. Hence, it is very difficult to keep frame-synchronizing the video and audio data. Consequently, regarding that two tracks might be independent of each other, it will be impossible to synchronize both data in the case of very large time lag. We solved this problem with adjusting the rotation phase of the video head by the method of trial and error. To synchronize audio and video frames was one of the most difficult problems on using the VTR. The degree of synchronization for a large extent should be related to the efficiency in the processing procedure of data.

2.3 Correlating Process

2.3.1 Buffer Memories

A wire memory is used as a RAM (Random Access Memory) which stores temporarily the reproduced data from the VTR (TOAMCO VR-489DR). The specifications of the wire memory are shown in Table 3. This wire memory is chosen by the following reasons:

(1) One word of the wire memory has 18 bits. The host computer NEAC 3100 used for the data processing in our VLBI system has also the same word structure.

(2) The cycle time of this wire memory is fast enough to store the data train from the VTR with the speed of 4 Mbps.

Table 3 Electronic specification of wire memory (HS-600E)

Memory device	woven plated wire memory
Memory capacity	4 k words × 18 bits
Cycle time	write cycle 600 nsec
	read cycle 600 nsec
Access time	300 nsec
Access mode	random access
Interface level	TTL, normally low
	"0" +2.4 --- +4.5V
	"1" 0 --- +0.5V

2.3.2 Correlation of Data at Two VLBI Sites

We designed this correlator to be carried out in hardware or software. Fig. 19 shows the correlation process in the case of hardware. The core memory of the host computer NEAC 3100 stores the one frame of data bits reproduced from VTR tape taken at Kashima through the course of the wire memory. Then wire memory stores the data taken at Yokosuka.

The corresponding bits of a word from both memories are fed to exclusive-NOR gates and the outputs are stored in the 8 bits binary counters. The process I/Os of NEAC 3100 collect the integrated cross-correlation data.

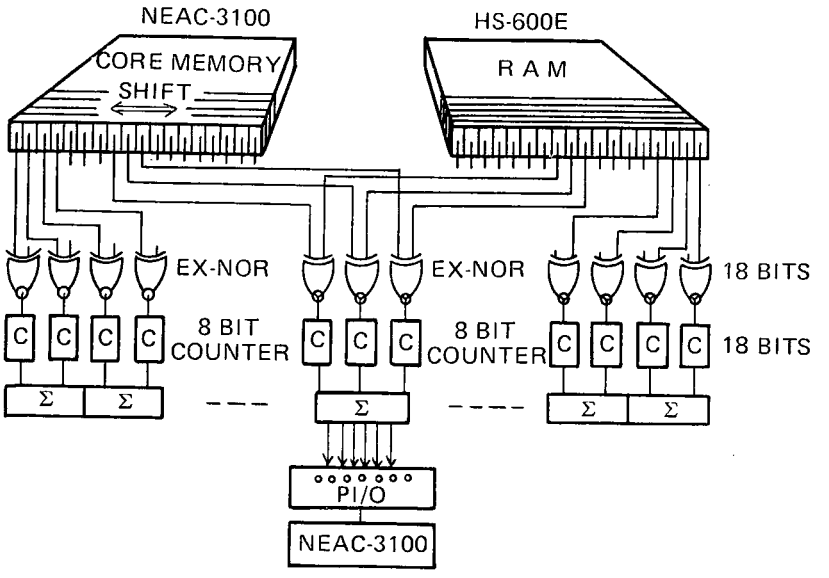

Fig. 19 Schematic illustration of bit-parallel and word-serial correlation

In general the cross-correlation r between the two sets of n data (x_i, i=1,...,n) and (y_i, i=1,...,n) is given by the next expression,

$$r = \frac{\sum_{i=1}^{n} (x_i - \bar{x})(y_i - \bar{y})}{(n-1) S_X S_Y}, \quad \cdots\cdots (7)$$

where S_X, S_Y : standard deviation of x, y around the mean value,
$\bar{x}$, $\bar{y}$: mean value of x, y.

In our case these sets are random variables, i.e.,

$$\bar{x} = \bar{y} = \frac{1}{2}, \quad \cdots\cdots (8)$$

and

$$S_X = S_Y = \frac{1}{2}\sqrt{\frac{n}{n-1}}. \quad \cdots\cdots (9)$$

We can modify the Eq. (7) and get the next equations

$$\begin{aligned} r &= \frac{4}{n}\sum_{i}^{n} (x_i - \frac{1}{2})(y_i - \frac{1}{2}) \\ &= \frac{4}{n}[\sum_{i}^{n} x_i y_i - \frac{1}{2}(\sum_{i}^{n} x_i + \sum_{i}^{n} y_i) + \frac{n}{4}] \quad \cdots\cdots (10) \\ &= \frac{4}{n}\sum_{i}^{n} x_i y_i - 1 \end{aligned}$$

The first term of Eq. (10) is the scaler products of two sets (x_i) and (y_i), and these products are equivalent to AND operation as shown in Fig. 20(a). However, exclusive-NOR

x_i \ y_i	0	1
0	0	0
1	0	1

(a)

x_i \ y_i	0	1
0	1	0
1	0	1

(b)

x_i \ y_i	−1	1
−1	1	−1
1	−1	1

(c)

Fig. 20 True value table of (a) AND, (b) exclusive NOR, and (c) arithmetic product

logic used in our system improves the efficiency of the correlator. The operation of an exclusive NOR gate is shown in Fig. 20(b), in which, if we substitute 0 for −1, we can get alternative table as Fig. 20(c). This new table instructs us that the correlations by exclusive NOR logics coincide just with the arithmetic products[10]. In this case we get

$$\bar{x} = \bar{y} = 0 \quad \cdots\cdots (11)$$

$$S_X = S_Y = \sqrt{\frac{n}{n-1}} \quad \cdots\cdots (12)$$

Then, Eq. (7) is reduced to a simpler form as

$$r = \frac{\Sigma x_i y_i}{n} \quad \cdots\cdots (13)$$

Comparing Eq. (10) with (13), it is seen that the efficiency of correlation is improved four times by exclusive NOR operation and also offset bias appeared in Eq. (10) is vanished in Eq. (13).

2.3.3 Software of VLBI Correlation

The program named VLBPRO is developed for VLBI correlation processing. The VLBPRO is divided into two subprograms. Those are the main routine and a subprogram named BITLPO for bit-alignment check.

The main routine controls the correlator which processes the VTR data at two stations of VLBI system, and also supervises the data transport from the correlator to NEAC 3100. The subroutine BITLPO monitors the bit alignment in the core memories and registers through the operation of correlation.

(1) Main routine

Fig. 21 shows the simplified flow chart of the main routine. The main routine is started by reading the parameters and the identification codes which control the operation of correlation. Those are shown in Table 4.

As the main routine is proceeded to STEP 1, the data processing of Kashima site is initiated. After the VTR on which the Kashima tape is loaded is started by the computer command, data in one frame which is previously selected by operator are written on the wire memory at the speed of 4 Mbps. The correlator cyclically checks and rewrites the contents of RAM, until the time code of that data coincide with the time appointed by operator. As soon as the correlator detects that the time code come to the previously given value, the contents of wire memory are latched and flag is sent to the NEAC 3100.

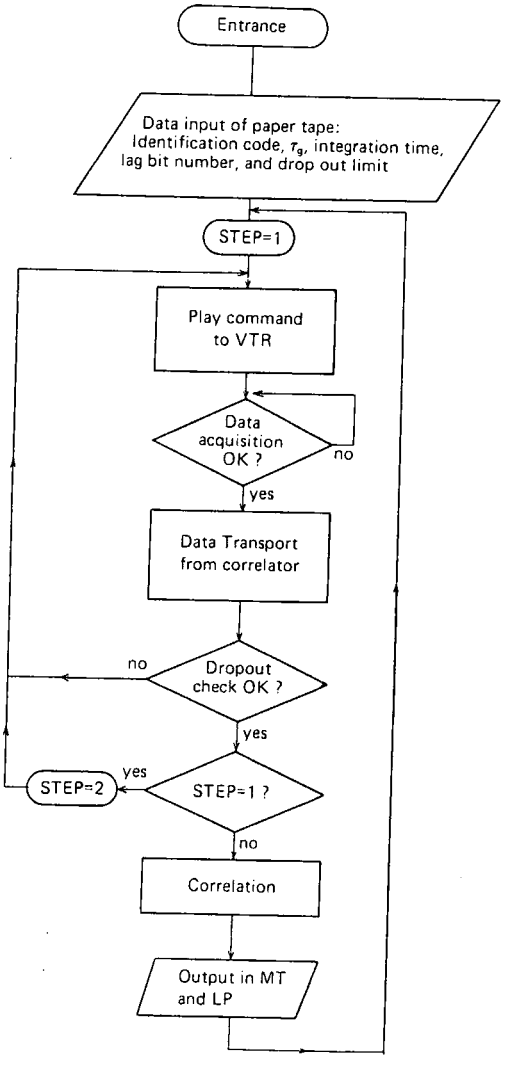

Fig. 21 Simplified flow chart of VLBPRO main routine

Table 4 Input parameters through photo-tape reader

Parameter	Function	
τ_g	geometric delay	(unit; sec)
T	integration time	(unit; word)
L	shift lag-number	(unit; bit)
D	limiting word-number to escape from dropout check routine	(unit; word)

The NEAC 3100 writes the latched data on its own core memory or mass storage such as DISC or MT.

The data in one frame is so large (about 66,000 bits) that the transports are carried out with the synchronous sequences of the commands and answers between the correlator and the host computer repeatedly.

The main routine checks the core data whether some dropouts of the bit alignment exist or not. When there is no dropout in the data, the correlator goes forward to the next step. But when there are some dropouts in the data, the correlator repeats the same process of STEP 1, until the check of dropout is judged to be good.

At the next step, the parameter STEP is set to the value two, and the reproduced data of VTR at Yokosuka site are processed as the same manner as the STEP 1. The similar check procedure of dropout is done on STEP 2.

After the dropout check for data taken at both antenna site is done completely, the correlation using exclusive NOR starts immediately. Setting two parameters, namely, the correlation integration time and the maximum lag numbers of bit-shift, we can correlate two data with selected format. We usually set the integration time and the lag numbers as 450 micro seconds and 36 bits respectively. The results by this process are transferred to magnetic tapes and a line printer.

(2) Subroutine BITLPO

We can utilize the subroutine BITLPO when the correlator and the host computer are in the wait loop or in the answer routines. The function of this subroutine is very useful to check the dropout at a glance and to make up the complicated hardware-software mixed system.

Subroutine BITLPO has the following three functions.

(a) Monitoring of registers

Subroutine BITLPO enables us to monitor the eight registers shown in Table 5. SC is

Table 5 Monitoring resisters of BITLPO

Register	Function
SC	Return address from BITLPO
ANS	Answer backs (see Table 6)
X1	Main routine index register
X2	Dropout routine index register
X3	Memory reading counter
X4	Integration counter
X5	Bit shift counter
DN	Dropout limiting register

the address of the main program and it also corresponds to the return address from BITLPO. ANS shows the steps of the answer routines. The main program has seven steps of the answer routines which are induced by answer backs from the correlator corresponding to the commands from the computer, and user can know the situation of the link connecting the two subprograms and connecting the process I/Os and of the correlation itself at user's

disposal. Table 6 shows the functions of the seven steps of the answer routine mentioned above.

Table 6 Answer-backs of the correlator corresponding to the commands from the computer NEAC 3100

Answer back	Function
A0	CPU run/wait control
A1	VTR servo synchronization
A2	End answer of RAM data writing
A3	Start answer of data transport to CPU
A4	Start answer of data transport to correlator
A5	End answer of correlation
A6	End answer of one sequence

(b) Passive and active wait loop

The selection of seven answer-backs at the entrance of BITLPO subroutine determines the next operation of the correlator. When answer-back is "off", the correlator goes into the wait loop and has some functions to monitor the eight registers mentioned in (a) and we call this mode as passive wait loop.

Active wait loop has higher priority over the passive one. When the sense switch 0 of the computer is on, BITLPO routine is in another mode of wait loop, and we call this mode as active wait loop. We can use the monitoring function in the same way as the passive one. A lamp on the computer panel is on in passive wait loop, but off in active wait loop.

(c) Function of core monitoring

The purpose of the core monitoring is to identify the bit alignment and the program sequence. When the program is in active or passive wait loop mentioned in (b), we can see the content of the core memory in binary representation.

The binary representation is more direct and clearer than the usual octal or hexadecimal representation, because we must monitor the one-bit sampling data.

In our VLBI system, bit error should be considered at two points of view. One type of error is dropout of the data, that is, dropout of timing clocks, which must be severer than another that is called bit inversion (see Fig. 22). No bit error is allowed in the former type, because even one bit of dropout make the resultant correlation quite useless.

On the other hand, a few bits inversion may make signal to noise ratio to be lower. In our case, up to two bits of conversion per one word with 18 bits can be allowed because the correlator makes no serious errors.

(d) Rejection of dropout

The clock pulses reproduced from the VTR data are fed into an L-C filter with fairly low Q. This provides a flywheel effect. Even if a clock transition is missed or an extra transition is inserted, the flywheel is neither decelerated nor accelerated, and we can be free from a few dropouts by this effect. But, it is very difficult to correct the larger series of dropout by this method, because, if we make Q of the filter higher, the clock pulse interval must be more uniform and the effect of the wows and flutters of VTR will be severer. Consequent-

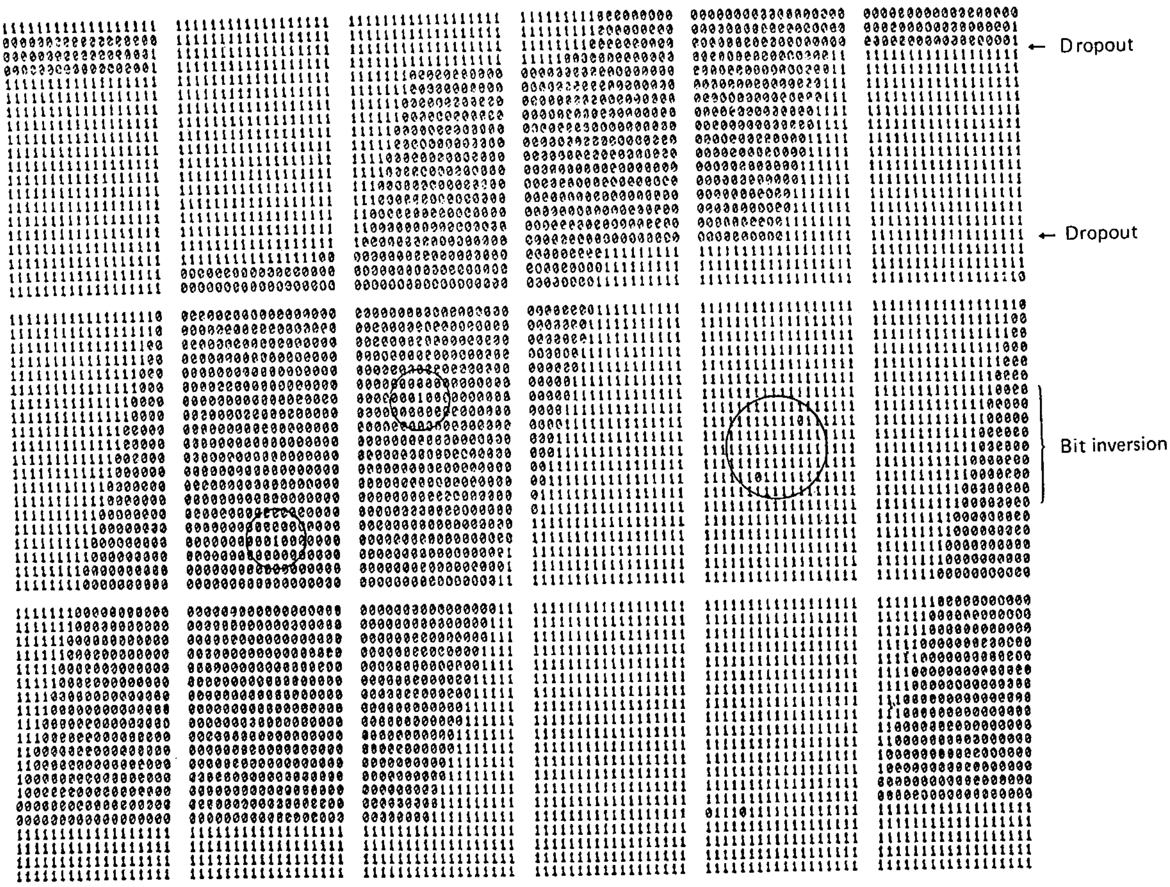

Fig. 22 Example of bit alignment check

ly, we set the next two conditions to the BITLPO software in order to reject the large series of dropout, one is high speed processing and another is independence of bit inversion.

We introduce the new concept "Hamming distance"(11) between the two word vectors to satisfy the above two conditions. The Hamming distance is defined as the number of bits which are not coincident with each word vectors. For instance, the Hamming distance D (W1, W2) between the two words W1 and W2 is defined as follows:

$$D(\vec{W1}, \vec{W2}) = 2, \qquad (14)$$

where $\vec{W1} = (010101\,1\,010100\,0\,10101)$

$\vec{W2} = (010101\,0\,010101\,1\,10101)$

In BITLPO, we adopt a criterion that, if $D \leqq 2$, dropout is dealt as none in the word, but if $D > 3$, as significant.

In Fig. 23, example of cross-correlation function with dropout is given.

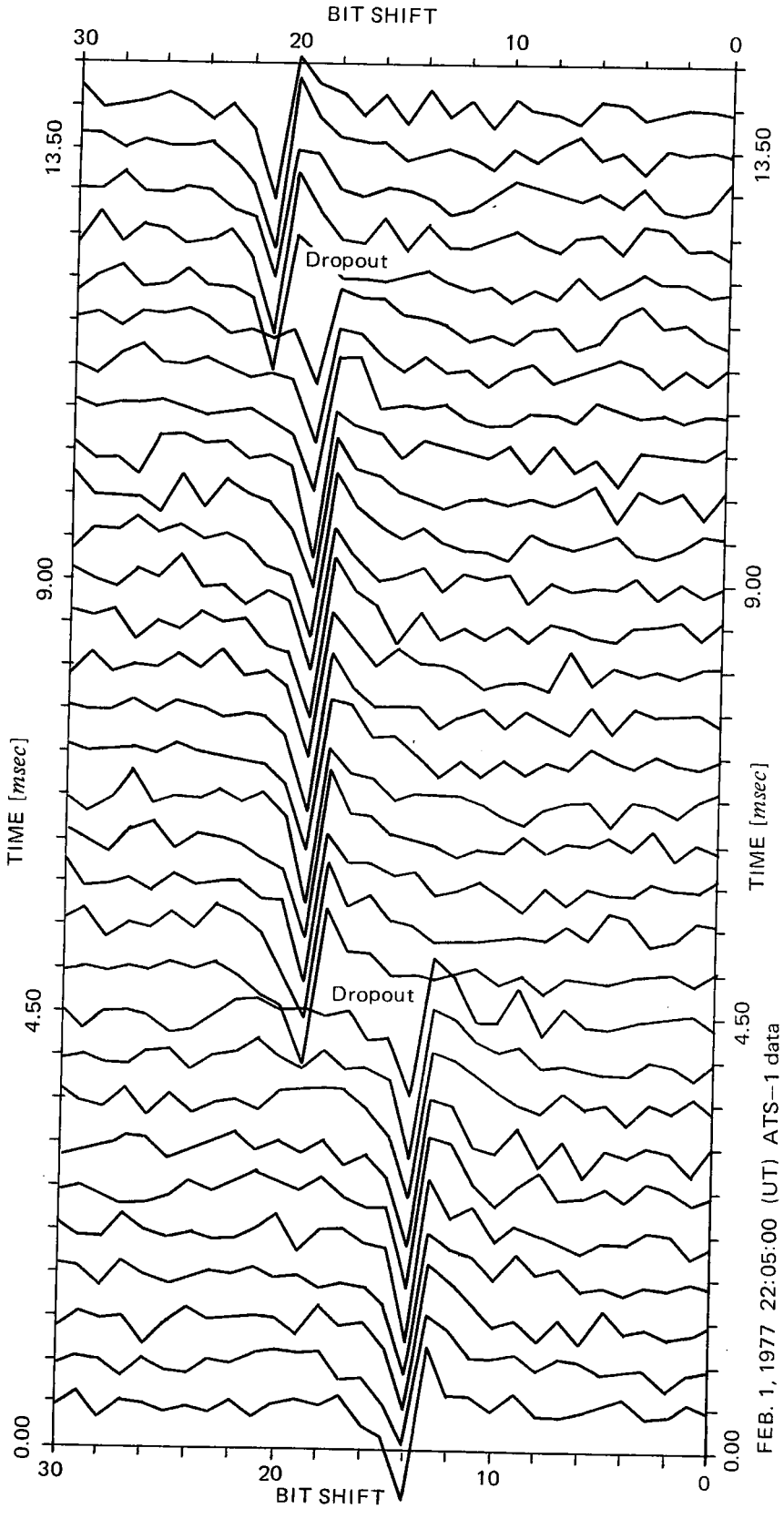

Fig. 23 Example of cross correlation function with the dropouts

2.4 Time Synchronization

It is desirable that the time and frequency standards used at both sites in the VLBI experiment are completely synchronized. However, it is impossible, in practice, to have the perfect synchronization for a long time duration, even if atomic standards were used for this purpose.

There are four methods to measure the time difference between two clocks separated over long distance with each other, as follows;

(1) Portable atomic clock,
(2) Loran C signals,
(3) TV synchronizing pulses and the color subcarrier,
(4) Time dissemination by satellites.

When the length of the baseline is short enough to receive the common TV signals, the TV signal provides fairly accurate time synchronization.

In our VLBI experiment between Kashima and Yokosuka, we used the TV synchronizing pulses emitted from the Tokyo Tower.

2.4.1 Arrangement of Atomic Clocks

A cesium standard HP 5061A equipped with a regular tube was used at each site respectively.

Just before the experiment, we brought the two standards together at Kashima, and compared mutually these two 5 MHz outputs by the accurate phase comparator. Considering the rate of change of time difference, we adjusted the difference in these two standards to set on zero in the midst of this experiment. Then we transported one clock to Yokosuka.

After the experiment we gathered both the clocks at Kashima again to check the comparison with linking by TV signals.

2.4.2 Method of Time Synchronization

The principle of time synchronization by TV signals are illustrated in Fig. 24[12]. A certain synchronizing pulse broadcasted from the TV tower is used as a reference pulse to compare two clocks.

The time difference, τ_e, between two clocks is given by the next equation

$$\tau_e = (R_1 - R_2) - (\tau_1 - \tau_2) - (d_1 - d_2), \quad \cdots\cdots\cdots\cdots\cdots\cdots\cdots\cdots \quad (15)$$

where R_1, R_2 : the times of reception of TV signal on the clocks to be compared,
τ_1, τ_2 : the propagation time of signals from the TV tower to the TV receivers,
d_1, d_2 : the delay time of signals in TV receivers at site 1 and 2, respectively.

$(\tau_1 - \tau_2)$ can be calculated from the geographic configuration between the transmitting and receiving points, and $(d_1 - d_2)$ is measured experimentally.

We used the portable clock method together with that of TV signal.

(1) Instruments

Fig. 25 shows the block diagram of the instruments for time comparison at the both sites of Kashima and Yokosuka. The time resolution of the used counter was 10 ns, and as the reference pulses we used the horizontal synchronizing pulses in the vertical blanking interval.

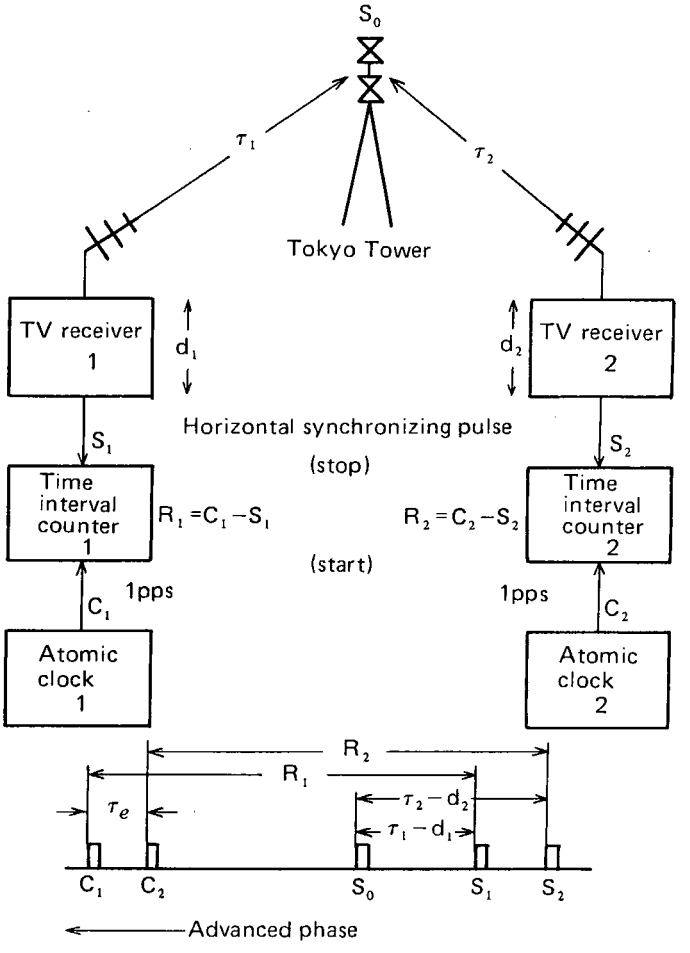

C_1, C_2: phase of second pulses of two clocks
S_0: phase of synchronizing pulse at TOKYO Tower
S_1, S_2: phase of synchronizing pulse at both sites
d_1, d_2: delay in respective TV receiver

Fig. 24 Principle of time synchronization by means of TV signal

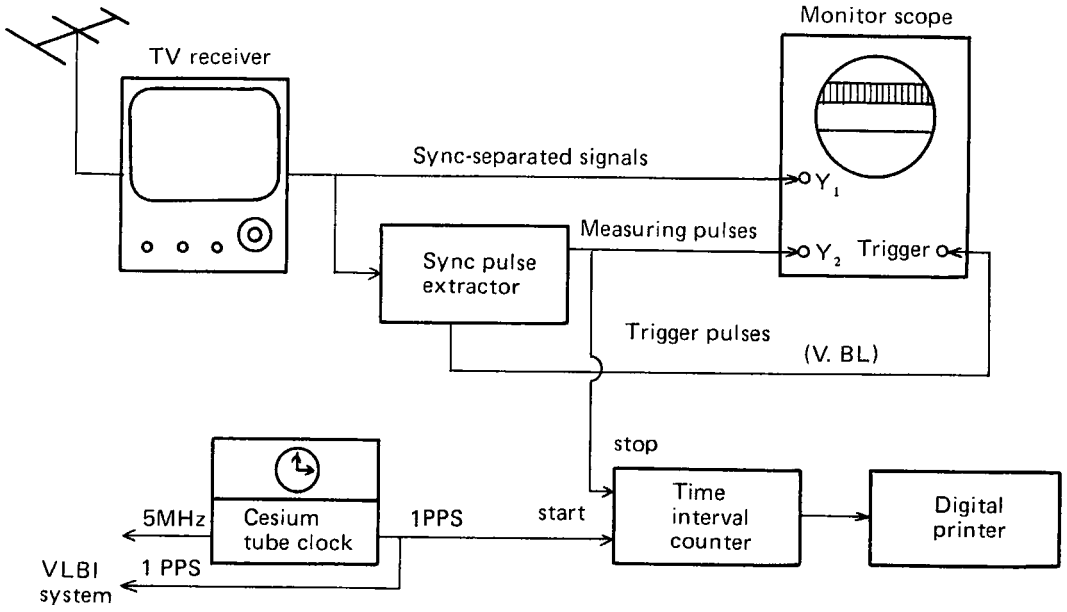

Fig. 25 Block diagram of time comparison by means of TV signal

(2) Difference of delay times

For the TV time synchronization, we must obtain the differences in propagation time and those of delay times in the receivers as mentioned above. In this experiment the portable clock method was used to decide these parameters before and after the experiment.

The resultant difference of delay times were 136.50 μs and 136.56 μs before and after the experiment respectively, and so we adopted the difference value of 136.53 μs as the average.

2.4.3 Result of Time Synchronization

During the experiment we made the simultaneous TV time comparison once a day at Kashima, Yokosuka, and Kokubunji. Thus the clocks at the both sites were monitored by the master clock of the RRL.

Fig. 26 shows the result of time synchronization, in which about 120 data of delay time averaged in each measurement are plotted.

The standard deviation of these data is ranging from 40 to 90 ns. There was no serious accident for the two clocks, but in the first half of the experiment there happened a rapid change of time difference. This change was apparently caused by the clock at Yokosuka, judging on each time difference referred to the master clock of the RRL in Fig. 27. It is probable that such a variation of frequency in the order of about 10^{-12} was introduced by the change of environmental conditions due to transporting.

Fig. 28 shows the residual apart from the linear part with time derived by the method of least squares for the clock comparison data by the direct and the TV pulse methods in Fig. 26. Fig. 28 tells us that the two clocks were almost in linear relation through the VLBI experiments if we allow the errors 0.15 μs.

We could grasp the difference of two clocks by the methods of portable clock and TV

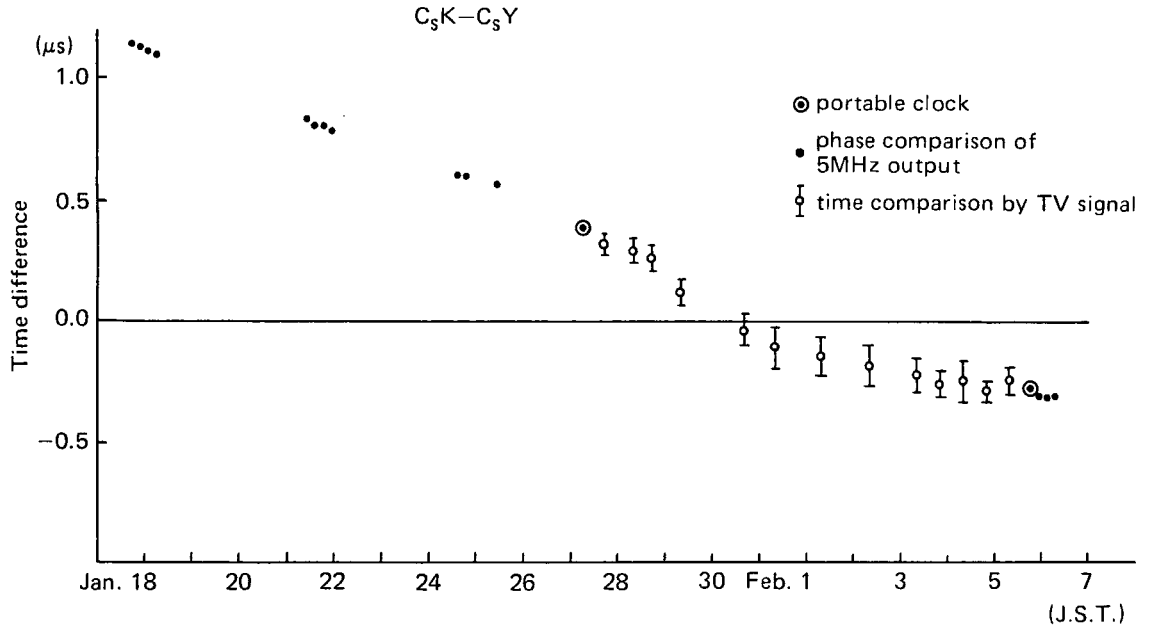

Fig. 26 Result of time synchronization by means of TV signal

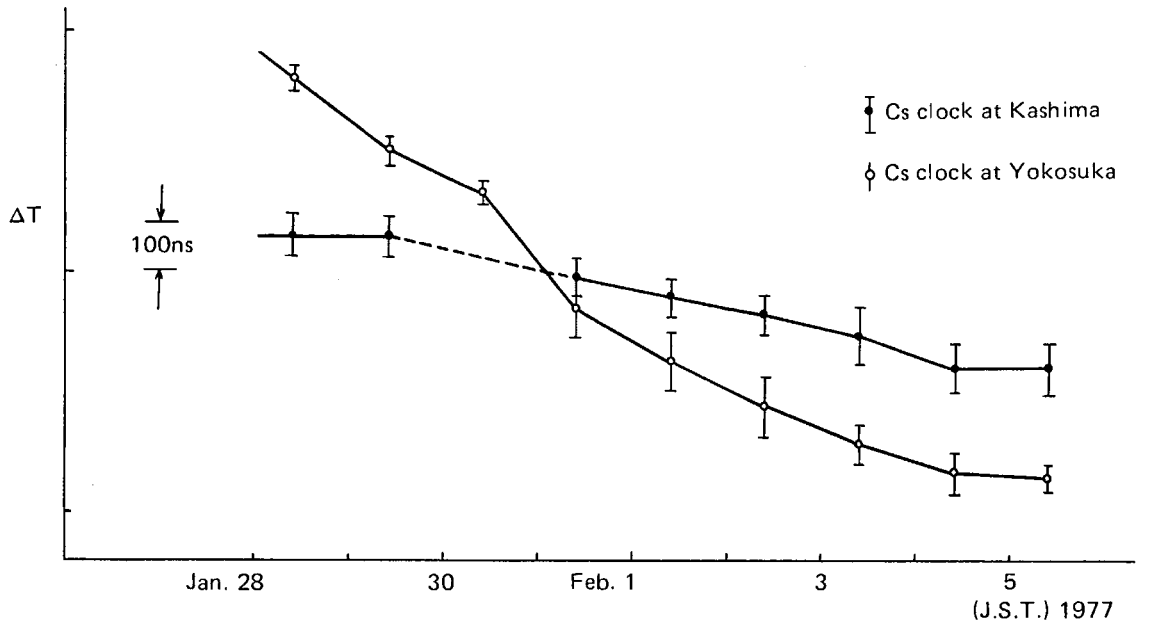

Fig. 27 Time difference referred to the master clock at Kokubunji

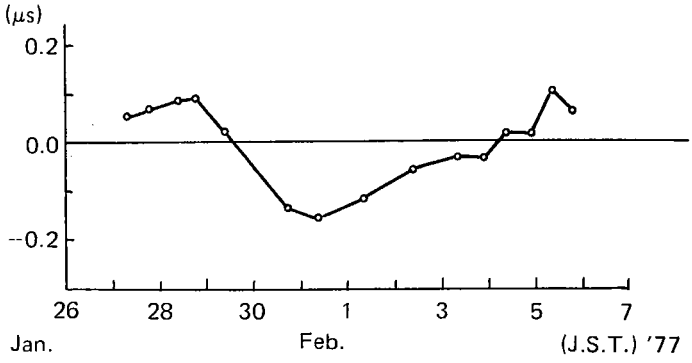

Fig. 28 Residuals on linear regression line derived from the least square method for the clock comparison data by the direct and the TV pulse methods in Fig. 26

synchronization in this experiments. However, if we need more accurate time synchronization, we must use the method of TV color subcarrier by which two clocks can be compared within errors 10 ns.

2.5 Measurement of Total Instrumental Delay

2.5.1 Instrumental Delay

In any VLBI experiments, it is important to know precisely the total instrumental delay (τ_i) because observed delay time always includes both τ_g (geometrical delay) and τ_i. To measure the time difference of wave front arriving at both antennas, a fixed reference point which is stationary independent of antenna motion must be established. We took that point at the intersection of the azimuth and the elevation axis. Thus, we must take account of the travel time of radio wave between main-dish and sub-dish, and the delay time of electric signal in the receiving system. The former is easy to know from the geometrical structure of the antenna. But, the latter can be known only by some measurements.

In our VLBI experiment, we set about 10 nsec accuracy as a goal in determining the instrumental delay.

2.5.2 The Delay in each Part

It is difficult to know the total instrumental delay τ_i by a single delay measurement at the respective antenna as a whole. So the measurement of total instrumental delay time at each site is divided into three parts. Those are:

A. Immovable part (e.g. parametric amplifier)
B. Movable part (e.g. I.F. converter)
C. The parts which are difficult to be measured (e.g. feeding system)

In Fig. 29, those parts are shown by dashed lines. At first, the method of measuring the part A is described. The instruments in this part are directly installed in the receiving system, so separate measurement of τ_i is needed to obtain the relative value. Fig. 30 shows the system to measure the delay in part A. As shown in Fig. 30(a), 4180 MHz signal (receiving band is 4180–4182 MHz) is fed to the parametric amplifier through a high speed PIN diode

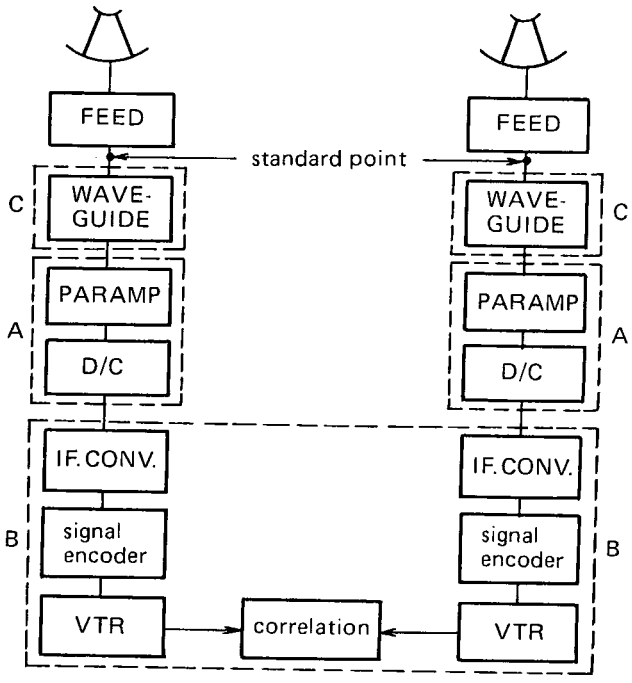

Fig. 29 Simplified block diagram of VLBI system for measurements of instrumental delay

modulator. The PIN diode is driven by a pulse generator with the fall time of less than 10 ns. 70 MHz I.F. output signal from the down-converter is connected to an oscilloscope by a cable 110 m long. The direct signal from pulse generator is fed to the another input of the oscilloscope. In this case, the sum of the delay time in the receiver τ_{ia} and the cable delay τ_{ib}, are measured as in Fig. 31(a). Next, the oscilloscope is brought to the down-converter and then the output of the pulse generator is connected through the 110 m cable as shown in Fig. 30(b). Then $\tau_{ia} - \tau_{ib}$ is measured.

From the measured delays, $\tau_{ia} + \tau_{ib}$ and $\tau_{ia} - \tau_{ib}$, we can obtain the instrumental delay τ_{ia} for the part A. In measuring the delay as mentioned above, we used an oscilloscope, because the time detected by time interval counter varied about 30 ns according to the signal voltage.

Secondly, the method of measurement in the part B is described. Since the bandwidth of the down-converted signal is only about 2 MHz, the accurate measurement of the delay in the part B is not expected by the same method as in the part A. As the rise and fall time in the waveform is inversely proportional to the bandwidth, it is difficult to determine the start and stop points in time interval measurement. Thus, the correlation technique was used and the relative delay for the part B was obtained (see Fig. 32).

The frequency-converted sky noise at 70 MHz was fed into both systems, and the recorded data in the VTR were correlated. Then the precise delay is determined by the slope of the phase spectrum (see in chapter 4). This method has the accuracy of 5 ns.

Thirdly, the delay in the part C is calculated theoretically in the geometrical size. We tried to measure this delay directly, but the feed system in Yokosuka station are very complicated, and many reflected waves were observed on scope, which made the measurement of

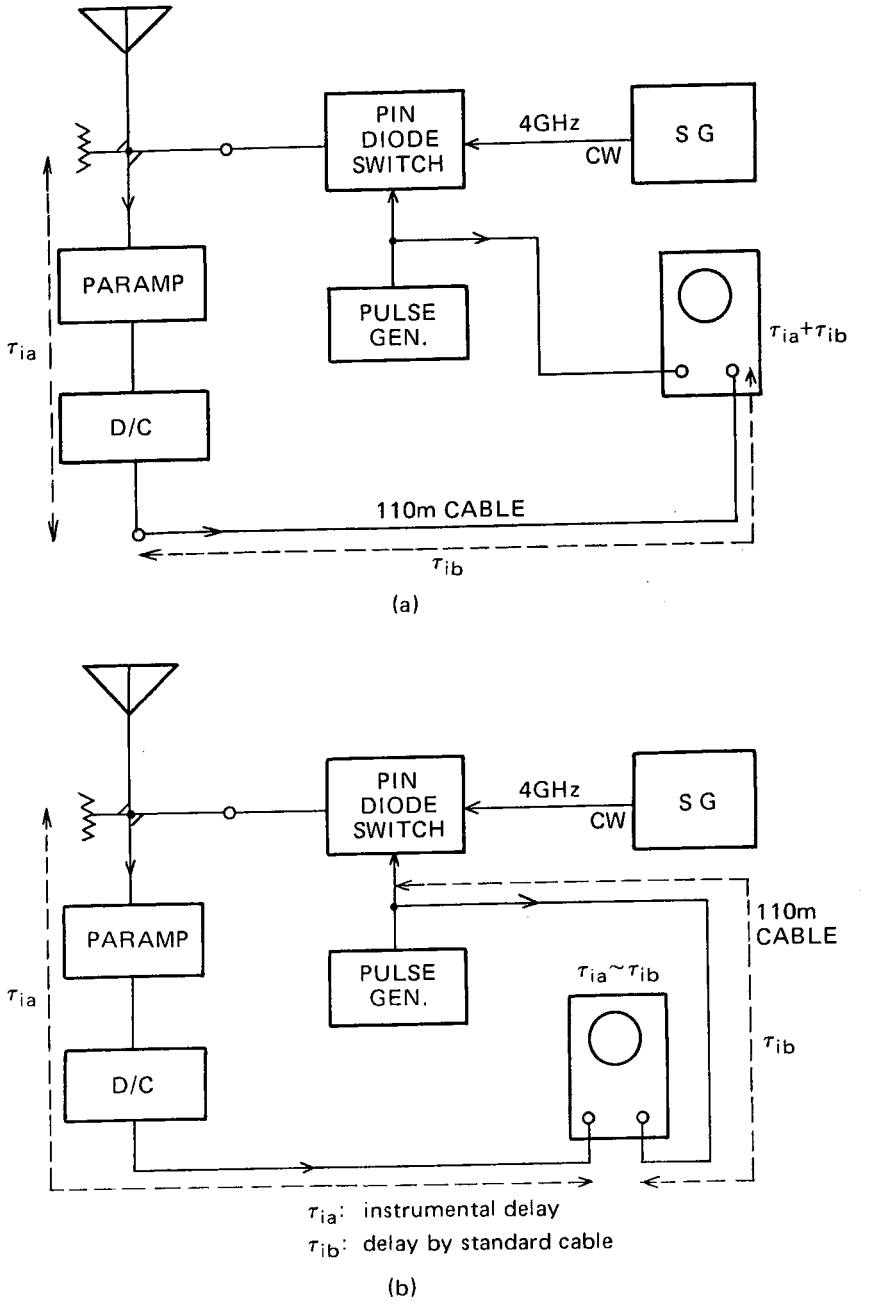

Fig. 30 Block diagram of the measurement of delay in part A
τ_{ia}: instrumental delay in part A, τ_{ib}: delay by the standard cable.

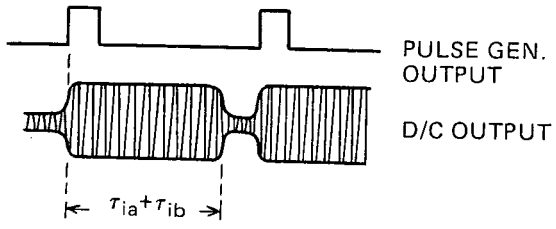

(a) Indication of $\tau_{ia}+\tau_{ib}$

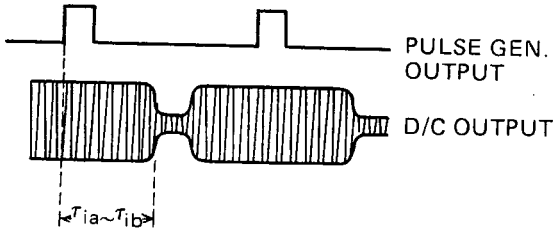

(b) Indication of $\tau_{ia}\sim\tau_{ib}$

Fig. 31 Oscilloscope indications in the measurement of delay in part A

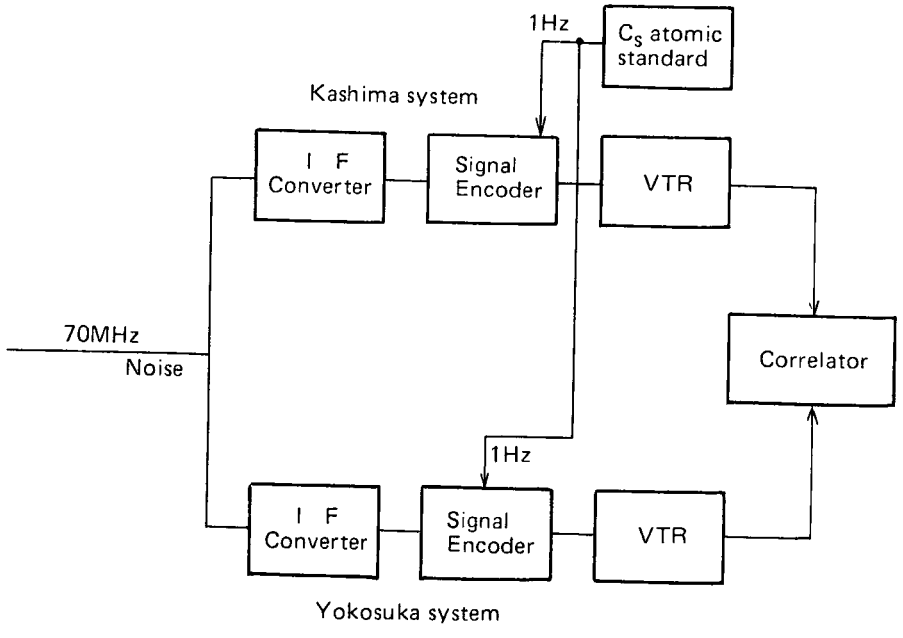

Fig. 32 Relative delay measurement in part B

delay impossible. On the other hand, the group delay characteristics in feed system are known well theoretically, and we can calculate the delay in part C in its size. The formula used here is

$$V_g = c\sqrt{1-(f_c/f)^2}, \quad \cdots\cdots (16)$$

where V_g : group velocity in the wave guide,
c : light velocity,
f_c : cut-off frequency,
f : radio frequency.

As mentioned in 2.5.1, the fixed reference point for measuring the instrumental delay is the intersection of azimuth and elevation axis. But, in Yokosuka antenna, the azimuth axis is separated by 1.8 m from the axis of main dish (see Fig. 3). Hence, the intersection of main-dish axis and elevation axis is used as the reference point. Then, it became easy to handle the data, because the total instrumental delay of this antenna system became constant independent of the antenna's motion. Though this point moves as the antenna is driven, the change of geometrical delay τ_g from the ideal case can be easily corrected for any direction of the antenna.

2.5.3 Result of Measurement of Instrumental Delay

The whole results are listed in Table 7. The error in the part A is estimated to be about 10 ns. The errors in the part B and C are about 5 ns. But, in the measurement of part A in Fig. 30, delay in the 110 m cable is obtained as 550 ~ 560 ns. This value is in good agreement with the theoretical one. So, this fact assured the accuracy of the delay measurement. In this experiment, we could not reach the goal of the accuracy less than 10 ns in delay measurement. However, accuracy of 0.1 ns will be realized in the near future by using other improved method such as comparison of delay with another simple standard system.

Table 7 Results of measurement of instrumental delay

	Section	Kashima	Yokosuka
A	Pre–amp.–IF conv. input	690 ns	320 ns
B	After input of IF conv. (relative)	139 ns	
C	Main refl.–std. point	56 ns	28 ns
	Std. point–Pre–amp. input	39 ns	50 ns

3. Experiment

3.1 Radio Sources

As mentioned in 1, ATS-1, Intelsat IV (F-8), and celestial bodies, 3C273B, 3C84 and 3C454.3 were utilized as the radio sources. Some features of each radio source are given in Table 8.

Table 8 Some features of each radio source used

Source	Intensity 1 f.u. = 10^{-26} w/m^2 Hz	Position	Other features
Geostationary satellite			
ATS-1	~ 6000 f.u. (−95 dBm)	Az: 95.2° ~ 108.4° El: 1.6° ~ 11.5°	Launched in Dec. 1966 by NASA
Intelsat IV (F-8)	~ 600 f.u. (−105 dBm)	Az: 131.5° El: 35.1° ±0.2°	Launched in Nov. 1974
Celestial radio source	(in Jan., 1977, at 4180 MHz)	(at the epoch of 1950)	
3C273B	45 f.u.	α: $12^h26^m33.2^s$ δ: 02°19′43.3″	Quasar
3C454.3	15 f.u.	α: $22^h51^m29.5^s$ δ: 15°52′54.3″	Quasar
3C84	38 f.u.	α: $03^h16^m29.6^s$ δ: 41°19′51.7″	Radio galaxy

(1) ATS-1

ATS-1 is the geostationary satellite launched by NASA in December 1966. We asked NASA to make commands from Rosman earth station, N.C., U.S.A., in order to enhance the satellite noise. The command was to switch on two TWTs in the transponder No. 2 for 4178 MHz at FT (Frequency Translation) mode. The reception of ATS-1 satellite noise were made every three hours from 13^h (U.T.) Feb. 1 to 13^h (U.T.) Feb. 2, and the same hours from the 3rd to the 4th of February.

The equivalent flux density of ATS-1 was more than 6000 f.u. or about −95 dBm (1 f.u. = 10^{-26}W/m^2·Hz), and integration time of only 0.45 ms corresponding to 100 words, was enough to detect a peak of cross-correlation.

At each measurement data, recording on the VTR was made for 10 min at the antenna direction of "on" satellite, and for 2 min of "off" satellite. During the reception of ATS-1, auto tracking by 4195 MHz beacon were utilized, as well as the program tracking at Kashima. On the other hand, only the program tracking was used at Yokosuka.

As the elevation of the satellite was so low as 1.6° ~ 11.5°, phase scintillation of the radio wave from the satellite might be detected(3).

(2) Intelsat IV (F-8)

The Intelsat IV (F-8) was launched on 21 November 1974 on a geosynchronous orbit above the Pacific Ocean. The frequency band of 4180 to 4182 MHz was included in the reserved TV channel. TWT in that satellite was always on, and the command from the earth station was not necessary. The apparent motion of the satellite was limited within 0.2° (about 131.5° in azimuth and 35.4° in elevation), which means almost being at rest.

The intensity was about 600 f.u. (about −105 dBm) as much as that of Tau A. We used this source to detect the first cross-correlation at the beginning of this VLBI experiment. The procedure of the data reduction was almost the same as that of ATS-1 except integration time, so any figures about this satellite are not shown here.

(3) Celestial radio sources

It is desired that the radio source as a standard of direction might be apparently small in size and strong in intensity. The apparent angular size of the celestial radio source must be smaller than the width of 0.12″ in fringe, which is formed by the configuration of Kashima and Yokosuka baseline (121 km) with 4180 MHz frequency. From these points of view, we selected 3C 273B, 3C 454.3 (quasars) and 3C 84 (radio galaxy) in this experiment. By this time, only the data of 3C 273B has been processed. The total intensity of 3C 273B was about 45 f.u., but correlated flux might be about 30 f.u., at the time of experiment.

The experiment was made once or twice every hour, and especially at the time when fringe rate was near zero.

3.2 Experimental Procedure

According to the schedule of receiving the sources, the VLBI experiment was performed every thirty min, as a rule.

The procedure in practice was follows:

1) Just before reception of the source, the clock faces were checked at Kashima and Yokosuka by phone, 2) after checking apparatuses in both sites the reception of signal and recording were started, 3) recording was made for the antenna direction of "on" and "off", 4) the system noise temperature was measured by the Y factor method, and 5) the stability of the local oscillator frequency was checked.

The system noise temperature had to be always monitored, because its increase deteriorated the degree of cross-correlation.

4. Data Processing

4.1 Theoretical Background of Data Processing

4.1.1 Geometrical Delay and Fringe Rate

In this section, the methods of VLBI data processing adopted in our experiments are briefly explained.

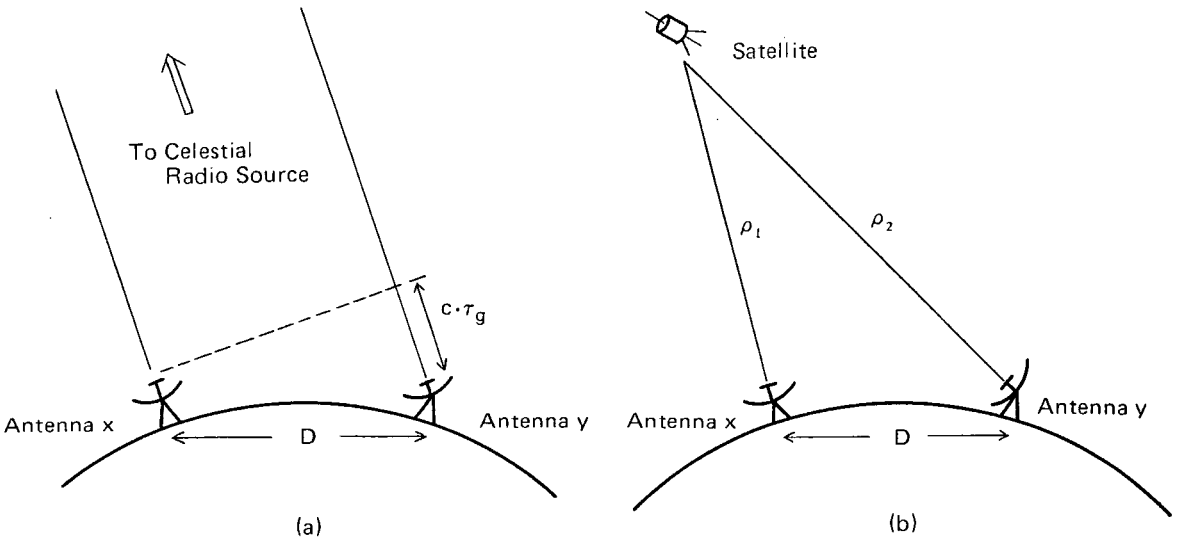

Fig. 33 VLBI configuration, (a) celestial radio source, (b) geostationary satellite

Assuming that radio waves from a very small point source are received at two antennas x and y, there will be a difference in the time of reception of the signal at the two antennas (see Fig. 33(a)). This delay τ_g (geometrical delay) for a celestial radio source is given by(13)

$$\tau_g = \frac{D}{c}[\sin\delta_b . \sin\delta_s + \cos\delta_b \cos\delta_s \cos(\alpha_b - \alpha_s)], \quad \cdots\cdots\cdots\cdots\cdots\cdots (17)$$

where
- c : the speed of light,
- D : the distance between two antennas,
- α_s : the right ascension of the source,
- δ_s : the declination of the source,
- α_b : the right ascension of the baseline vector,
- δ_b : the declination of the baseline vector.

In Eq. (17), the effects of the earth rotation, the earth tide, etc. during passage of time τ_g are neglected.

On the other hand, as shown in Fig. 33(b), the delay τ_g for a satellite is given by

$$\tau_g = (\rho_2 - \rho_1)/c, \quad \cdots\cdots\cdots\cdots\cdots\cdots\cdots\cdots\cdots\cdots\cdots\cdots\cdots\cdots\cdots\cdots (18)$$

where ρ_1 and ρ_2 are the slant ranges for the respective antennas. Eq. (17) shows that the delay τ_g changes with the earth's rotation. The sinusoidal variation in the geometrical delay τ_g with the period of a day corresponds to the second term in the parenthesis of Eq. (17), while the first term is measured as the bias in τ_g. Therefore, the distance D and the direction of the baseline in terms of the equatorial coordinate system are determined by several measurements of τ_g if the position of the celestial radio source, (α_s, δ_s), is already known.

One can find that the baseline can also be determined by fringe rate, Fr, i.e.

$$Fr = \omega\dot{\tau}_g, \quad \cdots\cdots\cdots\cdots\cdots\cdots\cdots\cdots\cdots\cdots\cdots\cdots\cdots\cdots\cdots\cdots (19)$$

where ω is the receiving angular frequency (RF frequency). In this case, unfortunately only equatorial component of the baseline is derived.

For the satellite, the orbital elements can also be determined by τ_g since ρ_1 and ρ_2 are concerned with orbital elements implicitly. The details are reported in the other paper on this issue by Kawase and Tanaka(2).

4.1.2 Procedure of Data Processing

Next, we try to explain the VLBI data processing applied in our experiments. The cross-correlation function Rxy (τ) between the two video signals after frequency conversion is given in the following form,

$$Rxy(\tau) = 2\cos[\theta + \omega^0(\tau_g + \tau_0) + \pi B\tau']\frac{\sin\pi B\tau'}{\pi B\tau'} \cdot B \quad \cdots\cdots\cdots\cdots (20)$$

$$\tau' = \tau_g + \tau_e + \tau_i + \tau_p + \tau = \tau_o + \tau,$$

where
- τ_g : the geometrical delay,
- τ_e : clock synchronization error,
- τ_i : instrumental delay,
- τ_p : delay produced by the wave propagation through the atmosphere,

θ : a phase difference between the two local oscillator frequency and produced by other cause,
ω^0 : angular local oscillator frequency
B : receiving bandwidth.

The Fourier transform of Rxy (τ) is shown in the following relation,

$$Sxy(\omega) = \int_{-\infty}^{\infty} Rxy(\tau) \exp(-i\omega\tau) \cdot d\tau$$

$$Sxy(\omega) = Sxx(\omega) \cdot \exp[i\Phi(\omega)] \quad \cdots\cdots (21)$$

$$\Phi(\omega) = \omega\tau_g + \phi,$$

where Sxx (ω) and ϕ are the power spectrum of the gaussian noise through the band-limited receiver and the phase delay except the one caused by the geometrical delay respectively. Of course, it is assumed that the receiving system at one antenna is the same as at another antenna. Although we can derive the delay τ_g from both equations (20) and (21), the next equation (22) is more convenient to evaluate τ_g, because τ_g is equal to $d\Phi(\omega)/d\omega$, i.e., the slope of phase spectrum which is defined as;

$$\Phi(\omega) = \tan^{-1}[\mathrm{Imag}\{Sxy(\omega)\}/\mathrm{Real}\{Sxy(\omega)\}], \quad \cdots\cdots (22)$$

$$\dot{\Phi}(\omega) = Fr.$$

The error of τ_g is estimated as

$$\Delta\tau_g = \Delta\phi/2\pi\Delta f, \quad \cdots\cdots (23)$$

where Δf is the effective bandwidth of the receiver and $\Delta\phi$ is the phase error in the bandwidth which mainly depends on signal-to-noise ratio. When the signals from a synchronous satellite are received, the phase error $\Delta\phi$ is sufficiently small for short integration time and $\Phi(\omega)$ does not change during this period. In our case, this error was about 5 ns since $\Delta\phi$ and Δf were several degrees and 2 MHz respectively.

On the other hand, the signal-to-noise ratio for celestial radio source is, in general, far smaller than that for satellite. Therefore, we would integrate Sxy (ω) corresponding to each short period over the long time interval, in order to reduce the phase error $\Delta\phi$. As mentioned earlier, the quantity of $\Phi(\omega)$ gradually changes at the rate of Fr, which is given in the equation (22). This means that the total or integrated cross-spectral function Soxy (ω) over the long time interval will vanish. In order to avoid this fact, "fringe rotation" or "fringe stopping" technique is applied to each Sxy (ω) obtained during short period, and then it is integrated over a longer time interval, i.e.,

$$Soxy(\omega) = \Sigma\, Sxy(\omega) \cdot \exp[-i\,\Phi_O(\omega)] \quad \cdots\cdots (24)$$

$$\Phi_O(\omega) = Fr_O \cdot \Delta t + \text{constant},$$

where Fr_O is the predicted fringe rate and Δt is the short integration time. It is obvious that the absolute value of the total or integrated cross-spectral function Soxy (ω) has a maximum when the predicted fringe rate coincides with the real one. Unfortunately, we can not know the real value of the fringe rate, since the small amounts of τ_p and τ_e always fluctuate. It is usual to assume various values of fringe rate and to evaluate Soxy (ω) corresponding to each

of the offset values. The offset that brings Soxy (ω) to the peak is chosen to be the correct value of fringe rate. After these estimations and corrections for τ_p, τ_e and τ_i, the geometrical delay can be determined.

4.2 Data Processing of Satellite

4.2.1 Satellite Orbit

We can compute the geometrical delay τ_g from the difference between both the slant ranges of two stations when the satellite's position is specified by the following orbital elements:

a = semi-major axis of the elliptic orbit;
e = eccentricity;
i = orbit inclination to the earth's equator;
$\tilde{\omega}$ = argument of perigee;
Ω = right ascention of the ascending node;
ν = true anomaly (cf. Fig. 34).

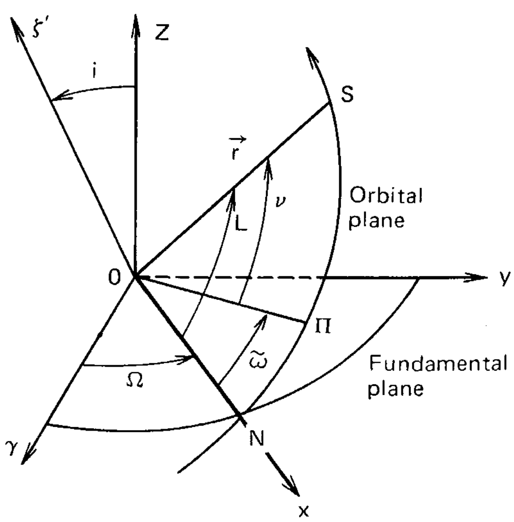

Fig. 34 Orbital elements: i = orbital inclination to earth's equator; $\tilde{\omega}$ = argument of perigee; Ω = right ascension of the ascending node; ν = true anomaly.

The slant range $\vec{\rho}$ from one station to the satellite is given by next equations

$$\vec{\rho} = \vec{r} - \vec{R}, \qquad (25)$$

where $\vec{r}$ is the vector from the earth's center to the satellite and $\vec{R}$ is that to the station shown in Fig. 35. We take the +X axis to pass through the ascending node and the +Z axis to pass through the earth's north pole. The +Y axis is orthogonal to both the X and Z axes. The satellite radius vector $\vec{r}$ is given by

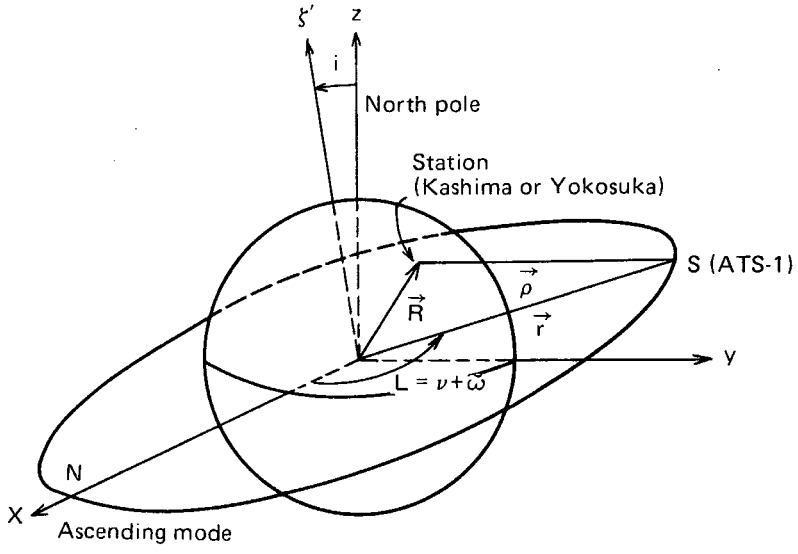

Fig. 35 Illustration of satellite position and earth station

$$\vec{r} = r\begin{bmatrix} \cos L \\ \cos i \cdot \sin L \\ \sin i \cdot \sin L \end{bmatrix}, \quad \cdots\cdots (26)$$

where L is the argument of latitude,

$$L = \tilde{\omega} + \nu, \quad \cdots\cdots (27)$$

and Kepler's First Law gives

$$r = a(1 - e^2)/(1 + e\cos\nu). \quad \cdots\cdots (28)$$

On the other hand, the station vector $\vec{R}$ is given by next equations

$$\vec{R} = R\begin{bmatrix} \cos\ell \cdot \cos(S\text{-}\Omega) \\ \cos\ell \cdot \sin(S\text{-}\Omega) \\ \sin\ell \end{bmatrix}, \quad \cdots\cdots (29)$$

where ℓ = geocentric latitude; S= local sidereal time.

The use of Eq. 26 and Eq. 29 gives the satellite range in the following equation,[14]

$$\rho = \{ r^2 + R^2 - 2rR [\cos\ell \{\sin^2\frac{i}{2}\cos[2L - (\Lambda - S)] + \cos^2\frac{i}{2}\cos(\Lambda - S)\} + \sin\ell \sin i \sin L] \}^{1/2}, \quad \cdots\cdots (30)$$

where Λ is the true orbital longitude,

$$\Lambda = L + \Omega = \nu + \tilde{\omega} + \Omega. \quad \cdots\cdots (31)$$

τ_g is derived from the difference between both two slant ranges and is given by the next equation

$$\tau_g = \frac{1}{C}(\rho_{YOKOSUKA} - \rho_{KASHIMA}), \quad \cdots\cdots\cdots\cdots\cdots\cdots\cdots\cdots \quad (32)$$

where c is the light velocity.

4.2.2 Data Reduction of ATS-1

ATS-1 is the geosynchronous satellite, but the maneuver of satellite control has been discontinued since 1976. Consequently, the satellite position of ATS-1 was changing to a fairly large extent. For example, the observed elevation angle is changing from 1.6° to 11.5° at Kashima.

Table 9 shows the typical observed delay data of ATS-1 according to time sequence.

Table 9 Reduction of delay data of ATS-1 from Jan. 31 to Feb. 3, 1977

Date (UT)	β_g	$\Delta\tau$	τ_m	τ_e*	τ_c
Jan. 31 13:04:10	1052bits	212ns	263212ns	628ns	263840ns
Feb. 1 13:05:20	1051	153	262903	554	263457
Feb. 1 16:05:20	960	239	240239	545	240784
Feb. 1 19:10:00	847	48	211798	536	212334
Feb. 1 22:06:59	794	192	198692	527	199219
Feb. 2 4:08:56	927	32	231782	508	232290
Feb. 2 10:05:59	1071	30	267780	442	268222
Feb. 3 13:13:58	1046	141	261641	408	262049
Feb. 3 16:12:00	952	68	238068	398	238466
Feb. 3 19:07:20	844	242	211242	388	211630
Feb. 3 22:06:20	794	223	198723	378	199101

β_g: Delay bit number, $\Delta\tau$: Residual delay by FFT, τ_m: Total delay,
τ_e*: Time synch. error τ_e + station bias, τ_c: Corrected value.

At first, we calculate the τ_g using Eq. 32 with the six orbital elements generated by KODS (Kashima Orbit Determination System) program developed by the staffs of Kashima branch. The delay bit-shift number β_g on the calculation of cross-correlation is given by next equation

$$\beta_g = \text{IFIX}\,(\tau_g/0.25), \quad \cdots\cdots\cdots\cdots\cdots\cdots\cdots\cdots\cdots\cdots\cdots\cdots\cdots\cdots \quad (33)$$

where the unit of τ_g is micro second and β_g is an integer because IFIX means the calculation where decimals are all cut off. The value 0.25 means one bit duration of 250 ns.

The maximum shift lag numbers and the integration time are set to the values of 32 bits and 450 μs respectively.

Table 9 also shows the sum of the station bias and time synchronization error. We calculated β_g by only from the theoretical value of τ_g, disregarding the sum.

The fast Fourier transform for 64 correlation coefficients was carried out to decide the residual delay $\Delta\tau$ smaller than 250 ns. Fig. 36 shows the method how to determine $\Delta\tau$ by means of a phase spectrum. The accuracy of the residual delay was about 5 ns by this

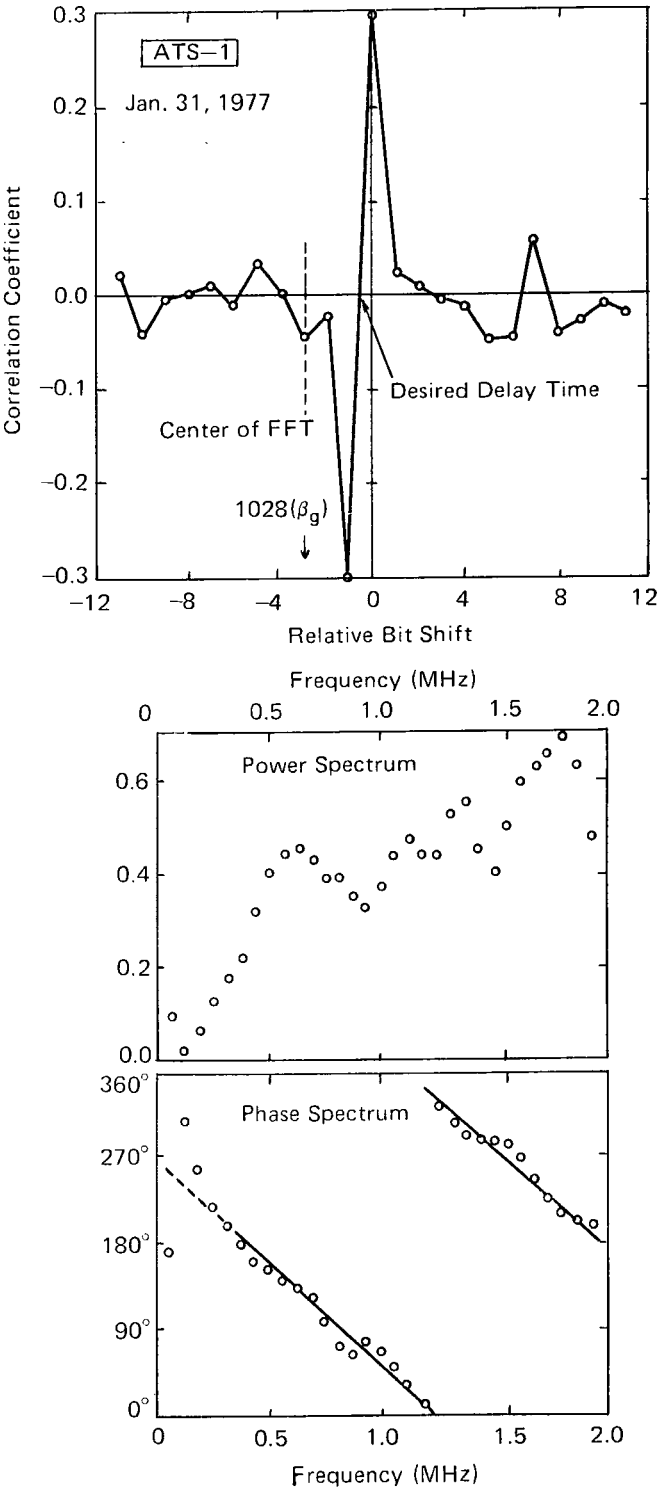

Fig. 36 Cross-correlation function of ATS-1, and its power and phase spectra. Residual delay is given by the slope of regression line of the phase spectrum.

method. In consequence, the value of the total delay τ_m measured by VLBI techniques is given by the next equation.

$$\tau_m = 250 \times \beta_g + \Delta\tau \text{ (ns)}. \quad \ldots\ldots\ldots\ldots\ldots\ldots\ldots\ldots\ldots\ldots\ldots\ldots \quad (34)$$

Table 9 shows the τ_m at each measured time and we obtained the corrected values τ_c considering the station bias and the time synchronization error τ_e.

These τ_c values were applied to the orbit determination of ATS-1, the results of which will be reported in the other paper of this issue[2].

4.3 Data Processing of the Celestial Radio Source 3C 273B

In this section the result of the observation of QSO 3C 273B using our VLBI system are reported.

As mentioned in section 4.1, "fringe stopping" shows one of the most important techniques in VLBI data processing for the detection of the celestial radio source and for the estimation of τ_g. In this method of data processing, we must make a precise prediction of fringe rate and total delay. Table 10 shows the various predicted parameters of our VLBI system and the radio source at $22^h25^m20^s$ (UT) on Feb. 2, 1977. Fig. 37 shows the integrated cross-correlation function for a duration of 0.3 sec for which the phase deviation caused by phase noise in two frequency standards would be within one radian. From this result, we could determine the "correct" geometrical delay τ_g, −328441 ns ±27 ns, which is different from the predicted τ_g by 3 ns.

Table 10 Predicted parameters of our VLBI system and radio source 3C273B at $22^h25^m20^s$ (U.T.) on Feb. 2, 1977

Kashima antenna	λ	140°57′15″.132	(SAO C-7)
	ϕ	35°39′45″.634	
Yokosuka antenna	λ	139°40′43″.383	(SAO C-7)
	ϕ	35°13′07″.101	
Baseline	α_b	1.36539756	(radian)
	δ_b	−0.58086469	(radian)
	D	120883.814	(m)
3C273B	α_s	$12^h27^m55^s.498$	
	δ_s	2°10′29″.902	
Geometrical delay	τ_g	−328438	(ns)
Station bias + time synch. error	τ_e	−527	(ns)
Fringe rate	Fr	−4.60	(radian/sec)

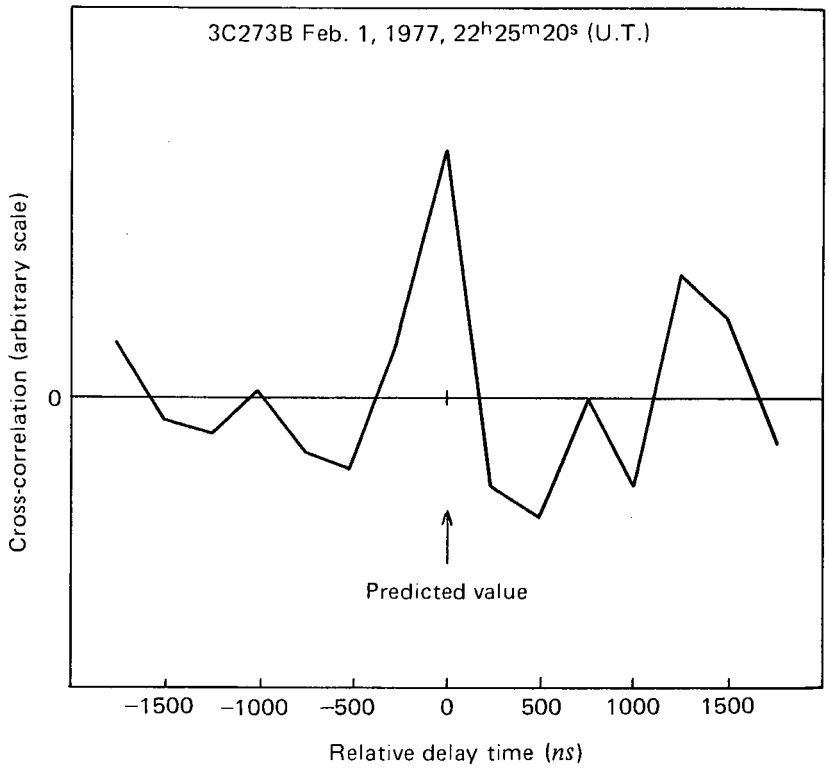

Fig. 37 Integrated cross-correlation function obtained from the data of 3C273B, in case the absolute value of Soxy (ω) is maximum

5. Discussion

As the detailed discussions for each part of the system are included in respective chapters, we summarize the principal parts of them in this chapter and add some items which are not referred to in the previous chapters.

(1) In spite of the separation by 1.8 m between the axis of main dish and the azimuth rotation axis of antenna at Yokosuka, it became easy to handle the data, because the intersection of main-dish axis and elevation axis is used as the reference point, and the total instrumental delay of this antenna system became constant being independent of the antenna's motion. Though this point moves as the antenna is driven, the change of geometrical delay τ_g from the ideal case can be easily corrected at any direction of the antenna (cf. 2.1.1 and 2.5.2).

(2) In the local oscillator system, we used the output of the Cs clocks with a regular tube as a frequency standard, and multiplication factors were 100 at Kashima and 10 at Yokosuka respectively, because different models of synthesizers were used. Even with the above things, at least a few seconds were assured at 4 GHz with the phase fluctuation within about one radian (cf. 2.1.2 and 2.1.3).

(3) We used VTR of rather handy type, VR 489DR, having memory for tremendous quantity of data and economizing cost performance. We remodeled the VTR to expand the bandwidth of video recording to fit the experiment. The points of remodeling were placed

on adopting the direct recording instead of the ordinary frequency modulation, and on the modeling of equalizing amplifiers and the recording current amplifiers. By this remodeling, the second harmonic of 4 MHz signal was recorded sufficiently, and we could make the most of the functions of the VTR, VR 489DR (cf. 2.2.1 and 2.2.7).

(4) Though dropout of data during the reproduction were occurred, we proceeded the data reduction with applying the conception of "Hamming distance" between two words, and confirmed the continuity of the time sequence of data (cf. in the section 2.3). Such dropout might be reduced, if we would record the data less densely by wider magnetic tape.

(5) The characteristics of the filter at the last mixer in the IF converter was slightly different from the ideal rectangular form. This caused an aliasing noise which occurred due to violation of Shannon's sampling theorem. One of the principal effects of this violation is as follows. In the phase spectrum, the gradient with respect to frequency, which determine the accurate residual delay $\Delta\tau$ are not constant between 0 and 2 MHz, and the frequency range in which the gradient show the true residual delay correctly, became narrow. However, we could, to some extent, make correction for the aliasing noise by detailed theoretical analyses.

We must also correct for the phase and power spectra in the band of the IF converter, which are shown in Figs. 38 and 39. These corrections were included in the software of the data reduction.

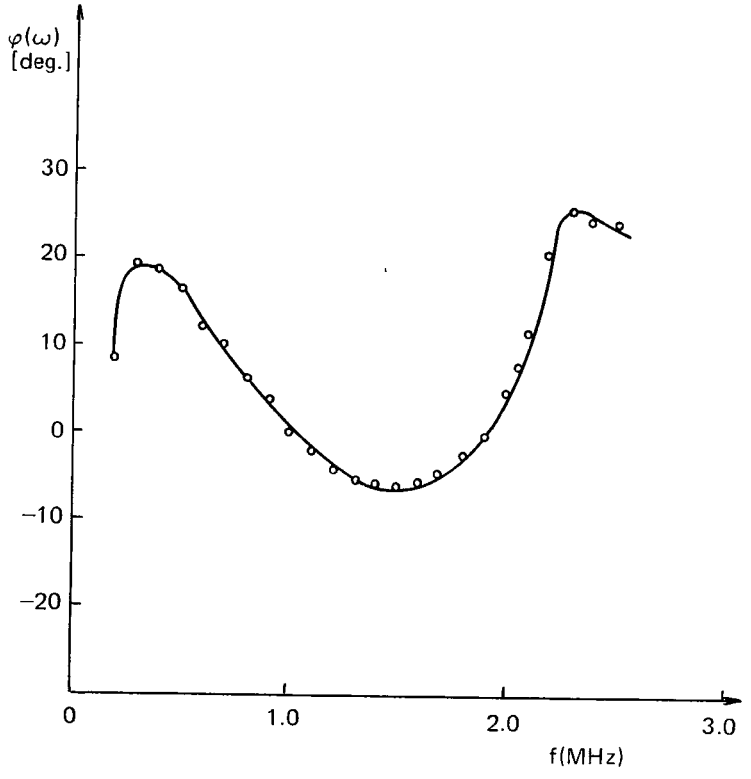

Fig. 38 Relative phase spectrum between the two I.F. converters

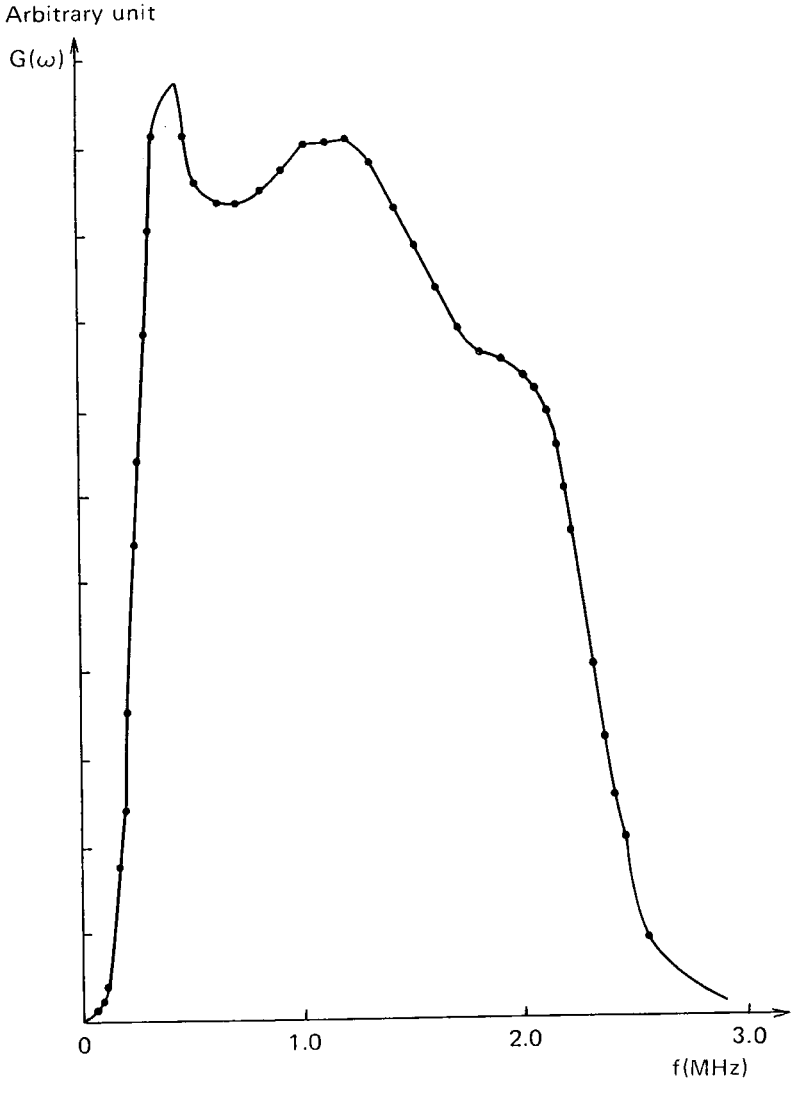

Fig. 39 Geometrical mean of the power spectrum of each I.F. converter

(6) We could grasp the difference of two clocks with the accuracy within about 0.1 μs by the methods of portable clock and TV synchronization in this experiments. However, if we need more accurate time synchronization, we must use the method of TV color subcarrier by which two clocks can be compared with within errors 10 ns (cf. 2.4.3)

(7) As for measurement of the instrumental delay, a fixed reference point which is stationary in spite of antenna motion was taken at the intersection of the azimuth and the elevation axis, and the measurings of total instrumental delay at each site are divided into three parts, A) immovable part, B) movable part, and C) the parts which are difficult to be measured. These parts were measured by the different method respectively. We could not reach the goal of the accuracy less than 10 ns in delay measurement. However, accuracy of 0.1 ns will be achieved in the near future by using other improved methods, e.g. using higher speed PIN

diode than in this experiment, applying the relative method for B) as far as possible, or by comparison of the instrumental delay with another simple standard system.

(8) In the process of the data reduction for celestial radio sources, integrated cross-correlation function for any 0.45 ms, during which variation of cross phase was less than one degree, was fourier-transformed into cross spectral function. Then, we repeated the phase rotation as many as about 600 times, according to the predicted fringe rate, and integrated the cross spectral function for a duration of 0.3 sec. Moreover, by changing the predicted value of fringe rate little by little, and by repeating the phase rotation and integration of the function, finally we obtained the correct value of fringe rate, for which the maximum value of the cross-correlation function was given. Then, we could determine the delay time for that case (for further reference cf. (15)). This process in the frequency domain needs much time, and it is desired that fringe stopping will be performed directly on cross-correlation function in time domain. In this case, if cross-correlation function is approximated by three levels, we need only changing the sign of the correlation function at one side across zero[16]. Even in the case of several levels, fringe stopping in real time can be carried out[15].

Other detailed discussions on the various parts of our system are given in the other papers[15].

6. Concluding Remarks

In our VLBI experiment, the following results were obtained.

(1) We achieved our purpose to establish the first VLBI system in Japan, though it was a preliminary experiment.

(2) By use of the VLBI data of geostationary satellite, ATS-1, we could determine the delay time with the error of 5 ns. If we could provide BPFs with sharp cutoff at 2 MHz in the last mixers, or made corrections for aliasing noises almost completely, the delay time would be determined more precisely.

The situation is the same as for the data of Intelsat IV (F-8), with the exception of more integration time.

(3) Orbit determination of geosynchronous satellites by the VLBI technique was also made with the use of the VLBI data of ATS-1 satellite noise, though this kind of analysis was not referred to in detail in this paper. We could obtain the reasonable values of orbital elements of ATS-1. The orbit determination method by VLBI data is very sensitive to satellite motion parallel to the baseline. This fact shows a feature as compared with the ordinary range and range rate method, which is sensitive to the range variation along the direction of line of sight. The computing program was "KODS" which was independently made at Kashima branch, RRL. For further reference, see the other paper presented on this issue[2].

(4) We could process the data of celestial radio source, 3C273B. For the celestial radio source, the relative phase changes rapidly together with the diurnal motion of the sources, and moreover, the flux intensity is fairly weak and need much integration time as compared with the satellite noise. So, according to the rate of path difference, i.e., fringe rate, we adjusted the relative phases of 3C273B data. In other words, we used fringe stopping technique before integration (otherwise correlation vanishes). After integration of 0.26 sec., we obtained the significant cross-correlation function (shown in Fig. 37). The difference between the obtained delay time and the predicted one was 2 ns $\pm$ 27 ns.

(5) From the cross phase spectrum, we could also determine the relative phase with the

error of about several degrees. As the wave length of receiving radio wave was about 7.2 cm, several degrees correspond to about 1 mm, and we could detect the phase scintillation of radio waves due to the earth's atmosphere. However, the fluctuation of local oscillator system, difference of the standard time, and the variation of propagation path are included in the observed change of the relative phase. So, it will be rather difficult for us to distinguish the phase scintillation due to the propagation media from the other causes.

(6) In the course of our VLBI experiment between Kashima and Yokosuka, time synchronization between two Cs atomic standards at both sites was made by using TV synchronizing pulses emitted from Tokyo Tower. We also used the portable clock method together with that of TV signal. The accuracy of the former was about 100 ns, and that of the latter was about 10 ns.

(7) The measurement of the total instrumental delay was also made together with the VLBI experiment, separating the whole system into three parts, A) immovable part (e.g. parametric amplifier), B) movable part (e.g. IF converter) and C) the parts which are difficult to be measured (e.g. feed system). The delay of the part A was measured by using a high speed PIN diode modulator, an oscilloscope and a standard cable. For the part B, the correlation technique was used and the relative delay was obtained by the slope of the phase spectrum. The delay in part C is calculated theoretically in the geometrical size. The error in the part A was about 10 ns, and those of parts B and C were about 5 ns respectively.

(8) For further VLBI applications, we are now planning a more accurate VLBI system with the time resolution of about 0.1 ns. Also, we will make the experiment together with the phase scintillation experiment by VLBI technique. 5 channels bandwidth synthesis experiment will be done between Kashima and Hiraiso branch (RRL) with real time data processing, as a part of the ECS (Experimental Communications Satellite) experiments in 1979. The baseline length is about 50 km, and the operating frequencies are 31.65 and 4.08 GHz. Bandwidth of each channel is 2 MHz, and total receiving frequency spans about 100 MHz.

Acknowledgement

The authors are grateful to Dr. H. Yuhara, and Dr. I. Kasuya, ex-directors of the Radio Research Laboratories, and Dr. K. Funakawa, the former director and Mr. K. Ikushima, the present Director of Kashima Branch, R.R.L., for their valuable contributions to promote this experiment.

They express their sincere thanks to the authorities of Yokosuka Electrical Communication Laboratory, Nippon Telegraph and Telephone Public Corporation, for providing the antenna system, and especially Dr. H. Fuketa, Mr. H. Shimada and Mr. H. Nishimoto of that Laboratory for their kind cooperation in this experiment.

They also express their hearty thanks to Mr. Richard Moore, ATS-1 Mission Operations Director at Goddard Space Flight Center, NASA, U.S.A., for the arrangement of making command at Rosman earth station, N.C., and to the staffs of that station for making command, to enhance the satellite noise from ATS-1.

They are also indebted to Professor N. Matsunami, of Tokyo Astronomical Observatory

and Dr. Y. Miyazaki, Geographical Survey Institute, Ministry of Construction, for their assistances in arranging software of this experiment.

This research was greatly supported by Mr. Y. Saburi, chief of Frequency Standard Division of the R.R.L., and by other staff members, Mr. Y. Yasuda, Dr. K. Yoshimura, Mr. J. Umezu, for their cooperation in measuring the stabilities of local oscillator system, and Messrs. S. Kobayashi, T. Sato and T. Ito in time keeping of Cs atomic standard and in time comparison by reception of TV signal.

Mr. C. Miki had taken part in configuring the VLBI system at the former stage of preparation.

References

(1) Kawajiri, N., Ojima, T., Kawano, N. and Takahashi, F.; "The first Domestic Basic VLBI System Developed in Radio Research Laboratories", Summaries of Papers, 1978 International Symposium on Antennas and propagation, Japan, B-3-4, Sendai Japan, Aug. 29–31, 1978.

(2) Kawase, S. and Tanaka, T.; "Orbit Determination of Geosynchronous Satellite by the VLBI Technique", J. Rad. Res. Labs., **26**, No. 119, March 1979.

(3) Ojima, T. and Kawano, N.; "Short Term Phase Scintillation through Troposphere", Summaries of Papers, 1978 International Symposium on Antennas and Propagation, Japan, C-9-3, Sendai Japan, Aug. 29–31, 1978.

(4) Allan, D.W.; "Statistics of Atomic Frequency Standards", Proc. IEEE, **54**, No. 2, Feb. 1966.

(5) Klemperer, W.K.; "Long Baseline Radio Interferometry with Independent Frequency Standards", Proc. IEEE, **60**, No. 5, May 1972.

(6) Ramasastry, J., Rosenbaum, B., Michelini, R.D., Frost, D., Ross, S. and Boornazian, A.; "Tracking of the ATS-3 Synchronous Satellite by the Very Long Baseline Interferometer (VLBI) Technique", GSFC Report X-553-72-290, July 1972.

(7) Van Vleck, J.H. and Middleton, D.; "The Spectrum of Clipped Noise", Proc. IEEE, **54**, No. 1, Jan. 1966.

(8) Rice, S.O.; "Mathematical Analysis of Random Noise", BSTJ, **23** and **24**, 1944 and 1945.

(9) Clark, B.G., Weimer, R. and Weinreb, S.; "The Mark II VLB System, Principles and Operating Procedures", Electronics Division Internal Report 118, NRAO, April 1972.

(10) Michelini, R.D.; "A One bit VLBI Recording and Playback System Using Video Recorders", SAO Symposium on VLBI, April 1970.

(11) Miyagawa, H., Iwadare, Y. and Imai, H.; "Coding Theory", Syokodo, Tokyo, pp. 15–16, 1973. (vernacular edition)

(12) Saburi, Y., Yasuda, Y., Kobayashi, S. and Sato, T.; "Precision Comparison of Time and Frequency by Means of TV Signals", Rev. Radio Res. Labs., **18**, No. 99, 1972. (vernacular edition)

(13) Rogers, A.E.E.; "Very Long Baseline Interferometry with Large Effective Bandwidth for Phase delay Measurements", Radio Science, **5**, No. 10, pp. 1239–1247, Oct. 1970.

(14) Slabinski, V.J.; "Variation in Range, Range-rate, Propagation Time Delay and Doppler Shift for a Nearly Geostationary Satellite", Communications Satellite Technology, Progress in Astronautics and Aeronautics, **33**, pp. 3–28, edited by P.L. Bargellini,

1974.

(15) "Special issue on Very Long Baseline Interferometery", Rev. Radio Res. Labs., **24**, No. 130, Sep. 1978. (vernacular edition)

(16) Whitney, A.R., Rogers, A.E.E., Hinteregger, H.F., Knight, C.A., Levine, J.I. and Lippincott, S., "A very-long-baseline interferometer system for geodetic applications", Radio Science, **11**, No. 5, pp. 421–432, May 1976.